J Comput Neurosci (2012) 33:301–319
DOI 10.1007/s10827-012-0387-7

Coupled left-shift of Nav channels: modeling the Na^+-loading and dysfunctional excitability of damaged axons

Pierre-Alexandre Boucher · Béla Joós · Catherine E. Morris

Received: 19 October 2011 / Revised: 25 January 2012 / Accepted: 12 February 2012 / Published online: 5 April 2012

Abstract Injury to neural tissue renders voltage-gated Na^+ (Nav) channels leaky. Even mild axonal trauma initiates Na^+-loading, leading to secondary Ca^{2+}-loading and white matter degeneration. The nodal isoform is Nav1.6 and for Nav1.6-expressing HEK-cells, traumatic whole cell stretch causes an immediate tetrodotoxin-sensitive Na^+-leak. In stretch-damaged oocyte patches, Nav1.6 current undergoes damage-intensity dependent hyperpolarizing- (left-) shifts, but whether left-shift underlies injured-axon Nav-leak is uncertain. Nav1.6 inactivation (availability) is kinetically limited by (coupled to) Nav activation, yielding coupled left-shift (CLS) of the two processes: CLS should move the steady-state Nav1.6 "window conductance" closer to typical firing thresholds. Here we simulated excitability and ion homeostasis in free-running nodes of Ranvier to assess if hallmark injured-axon behaviors—Na^+-loading, ectopic excitation, propagation block—would occur with Nav-CLS. Intact/traumatized axolemma ratios were varied, and for some simulations Na/K pumps were included, with varied in/outside volumes. We simulated saltatory propagation with one mid-axon node variously traumatized. While dissipating the $[Na^+]$ gradient and hyperactivating the Na/K pump, Nav-CLS generated neuropathic pain-like ectopic bursts. Depending on CLS magnitude, fraction of Nav channels affected, and pump intensity, tonic or burst firing or nodal inexcitability occurred, with $[Na^+]$ and $[K^+]$ fluctuating. Severe CLS-induced inexcitability did not preclude Na^+-loading; in fact, the steady-state Na^+-leaks elicited large pump currents. At a mid-axon node, mild CLS perturbed normal anterograde propagation, and severe CLS blocked saltatory propagation. These results suggest that in damaged excitable cells, Nav-CLS could initiate cellular deterioration with attendant hyper- or hypo-excitability. Healthy-cell versions of Nav-CLS, however, could contribute to physiological rhythmic firing.

Keywords Hodgkin-Huxley · Diffuse axonal injury · Myelinated · Arrhythmia · Neuropathic pain · Na/K-ATPase · Extracellular space

Action Editor: T. Sejnowski

P.-A. Boucher · B. Joós (✉)
Department of Physics, University of Ottawa,
150 Louis Pasteur,
Ottawa, Ontario K1N 6N5, Canada
e-mail: bjoos@uottawa.ca

P.-A. Boucher
e-mail: pbouc040@uottawa.ca

C. E. Morris (✉)
Neurosciences, Ottawa Hospital Research Institute,
Ottawa, Ontario K1H8M5, Canada
e-mail: cmorris@uottawa.ca

1 Introduction

A devastating aspect of traumatic brain injury is that even in the "penumbra", where the initial damage is mild and there is no axolemmal rupture, axon demise continues for hours and days (Smith et al. 2003). Saving the penumbral axons is a major but entirely unmet clinical goal; one impediment is that, while voltage-gated sodium channel (Nav) dysfunction is known to be a key factor, their sustained post-trauma "leakiness" is poorly understood. Mechanical insults (Wolf et al. 2001), like ischemic insults (Schafer et al. 2009), induce tetrodotoxin (TTX)-sensitive degenerative excitotoxic cascades; Na^+-loading occurs because of injury-modified Nav channel activity (Yuen et al. 2009; Wang et al. 2009). Elevated intracellular Na^+ concentration ($[Na^+]_i$) eventually stalls the Na^+/Ca^{2+} exchangers and as Ca^{2+}-extrusion fails, multiple intracellular $[Ca^{2+}]_i$-sensitive

processes over-activate, with ATP depletion and reactive oxygen species further exacerbating the damage (Stys 2004). Among the Ca-sensitive enzymes governing plasma membrane integrity are lipases, gelsolin, acto-myosin-regulating proteins, and calpain. Over-activate calpain destroys the spectrin skeleton that organizes Nav-rich axonal membranes, and in stroke models, calpain-cleaved spectrin fragments bespeak irretrievable axon damage (McGinn et al. 2009). What links mechanical (or ischemic or inflammatory) insult to lethal Nav channel leak? The attendant bleb-like degradation of the Nav-rich membrane, we postulate (Wang et al. 2009; Morris 2011a). A membrane bleb is a patch of bilayer that has lost its adhesion to membrane skeleton. Catastrophic blebbing is a feature of apoptosis, but blebbing also has less extreme manifestations. These include the benign reversible blebbing of ameboid crawling (Charras and Paluch 2008) and what is at issue here, namely injury-induced (and potentially reversible (Draeger et al. 2011)) damage (Morris et al. 2012a). Integral membrane proteins in damaged membrane regions will see bilayer structures that are fluidized, abnormally symmetric, thin, and laterally disordered. To activate at their normal physiological voltages, voltage-gated channels require normally-structured bilayer (Morris 2011c). In damaged membranes, they activate too easily, i.e., at abnormally hyperpolarized (left-shifted) voltages (Morris 2011a, b). Irreversibly left-shifted activation of Nav channels in bleb-like membrane, we hypothesized (Wang et al. 2009), underlies lethal Nav-leak in traumatized axons or ischemically-damaged (Schafer et al. 2009) axon initial segments.

Observations motivating this hypothesis include: 1) trauma causes blebbing of the Nav1.6-rich node of Ranvier axolemma (Maxwell 1996; Lorincz and Nusser 2010), 2) abrupt whole-cell stretch of Nav1.6-expressing HEK cells causes immediate TTX-sensitive Na^+-loading (Na^+-dye experiments (Wang et al. 2009)), and 3) oocyte-expressed Nav1.6 channels in progressively damaged membrane (pipette aspiration) show progressive, irreversible left-shift of activation and steady-state inactivation (availability), consistent with a progressive irreversible decrease of the energy barrier for Nav activation (Wang et al. 2009). Similar shifting occurs for Nav1.5 expressed in HEK cells (Beyder et al. 2010). Since Nav "inactivation particle" binding is kinetically coupled to the activation process, Nav window conductance, the steady-state product of activation and availability, left-shifts whenever activation shifts. Compared to healthy Navs in uninjured axolemma, Navs in adjacent damaged membrane would produce low-threshold "persistent I_{Na}" ("Nav-leak") resembling the pacemaker neuron "subthreshold persistent I_{Na}" described by Taddese and Bean (2002).

To simulate realistic coupling of inactivation to an activation process that generates a subthreshold persistent I_{Na}, Taddese and Bean (2002) use a many-state allosteric Markov model; in that model a Nav channel passes both persistent and transient I_{Na} because the inactivating particle binds weakly to the resting-state channel but strongly to the already-activated channel. It turns out that the minimally changed standard Hodgkin-Huxley model used here to mimic the shifted operation of damaged-membrane Nav1.6 channels can approximate this outcome, while being computationally tractable.

Axonal Nav1.6 channel transient I_{Na} underlies propagating action potentials (APs), but axons also show persistent or "non-inactivating" I_{Na} of uncertain provenance (Stys et al. 1993; Burbidge et al. 2002; Tokuno et al. 2003). Bostock and Rothwell (1997) reported a peripheral axon persistent I_{Na} resembling a Taddese-Bean subthreshold persistent I_{Na}. Persistent I_{Na} in the first node of central axons also appears to behave this way (Kole 2011).

A coupled left-shift (CLS) model of Hodgkin-Huxley (HH) activation/availability is used here to mimic traumatic Nav leak (Hodgkin and Huxley 1952). Our "damage-induced persistent I_{Na}" emerges from HH formulations by making m and h (the HH parameters for activation and inactivation) for the affected channels left-shift by the same number of millivolts. This mirrors experimental data (Wang et al. 2009) for Nav1.6-bearing membrane during mechanically-induced damage. There, activation and availability exhibit kinetic coupling both before and after trauma-induced left-shift. The experimental trauma decreases steady-state Nav1.6 I_{Na} near 0 mV; in our CLS trauma model, steady-state I_{Na} decreases near 0 mV (while increasing near V_{rest}). In stark contrast, the widely-held assumption is that increased "non-inactivating-g_{Na}" must be what underlies Nav-leak in trauma, ischemia, inflammation, etc. (e.g., Wolf et al. 2001; Monnerie et al. 2010). In that case, steady-state I_{Na} near 0 mV would always increase with trauma. However, for recombinant Nav1.6 (Wang et al. 2009) it seldom does so, but CLS is always observed with trauma. Because of this and because other consequences of CLS-based Nav-leak via otherwise normally-functioning Nav channels are not self-evident, we undertook this computational study.

Our initial goal was to test if CLS of Nav channel operation (Nav-CLS) could reasonably be expected to generate sufficient axonal Na^+-leak to dissipate the Na^+ gradients in myelinated axons within minutes or hours. To validate our system, we over-stimulated the intact system (with pumps included) while monitoring excitability-induced Na^+-loading followed by ion gradient recovery. Then, both without and with pumps, we characterized behaviors in minimally-stimulated and spontaneously active axon systems as the proportions of intact versus CLS-traumatized axolemma were varied. It emerged that Nav-CLS would be able to run the system down in minutes or hours (depending on CLS intensity), and that, in the process,

it would generate dysfunctional patterns of excitability. How I_{Na} abnormalities in trauma-induced peripheral neuropathic pain arise has been unclear (Kovalsky et al. 2009) so it was interesting that with pump activity included in our system, Nav-CLS yielded bursting behaviors such as occur in neuropathic pain and related ectopic excitation phenomena (Devor 2009). In any system, extracellular space magnitude unavoidably affects pump efficacy and we found that CLS-induced burst duration and frequency varied steeply with variations in extracellular volume.

While traumatic nerve injury was the context for modeling effects of Nav-CLS, our simulations could pertain to diverse situations of injury and/or excitable cell plasticity in which sub-populations of Nav channels exhibited CLS.

2 Materials and methods

This study uses electrical circuit models (Fig. 1) solved with in-house computer programs that build on the Hodgkin-Huxley (HH) model (1952) (the codes have been uploaded to the database ModelDB). The model has a transient Na^+ current (I_{Na} due to Nav channels), and a non-inactivating fast K^+ current (I_K due to Kv channels), plus an unspecified

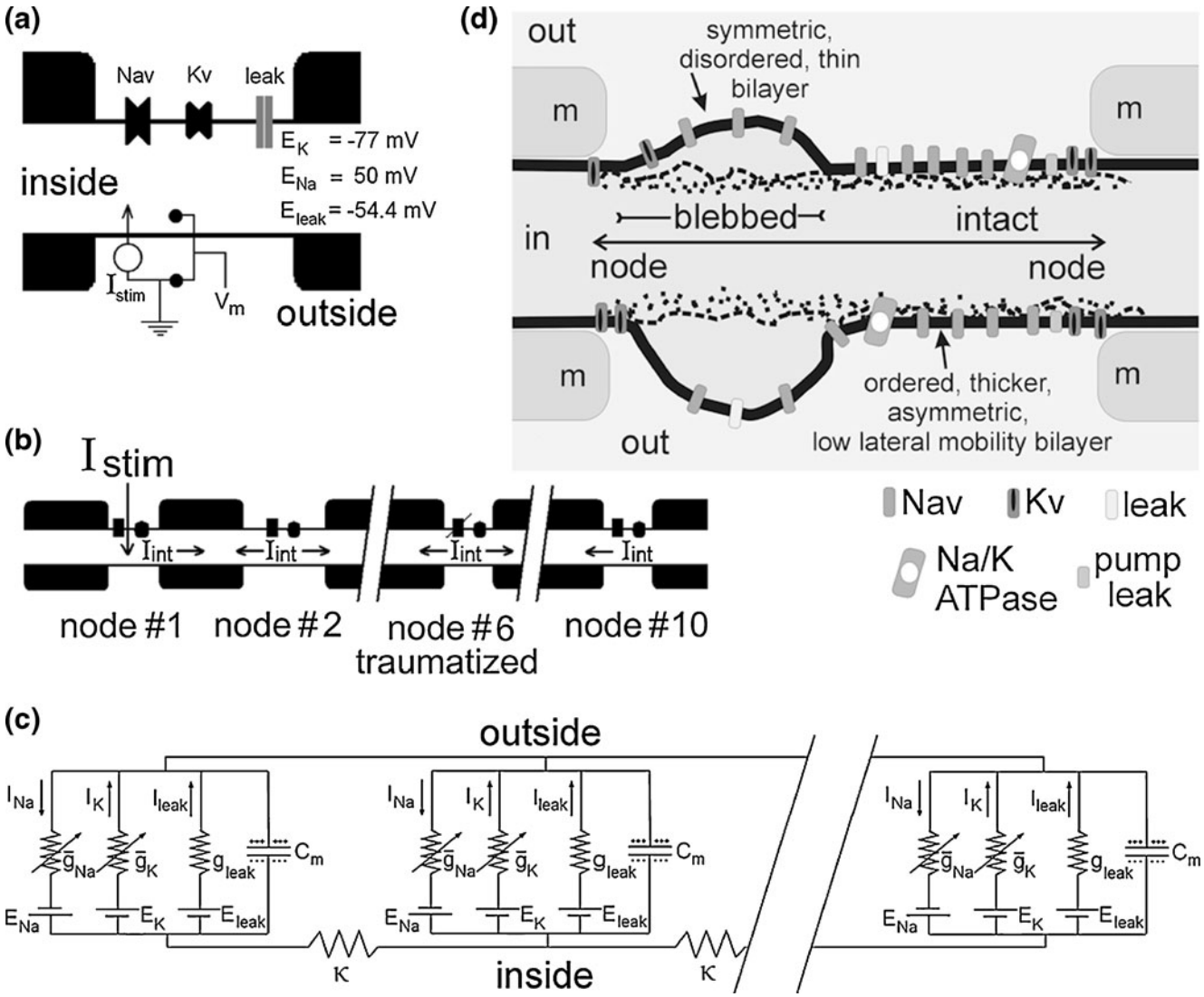

Fig. 1 Cartoons of models used for axon simulations. (**a**) Single node with conductances and fixed reversal potentials (mimicking fixed ion concentrations and short times, as per Table 1, single nodes). By contrast, when pump activity is added to the single node model, driving forces varied and inside and outside volumes are made explicit (as per Table 2); (**b**) For studying saltatory propagation, a ten-node myelinated axon was modeled, with one node (#6) given a specified CLS (of "X" mV) to a specified fraction of the total nodal g_{Na} (see Eq. (10) and accompanying text for explanation); (**c**) Equivalent circuit (3 nodes and 2 internodes depicted) for saltatory propagation (as noted under Table 1). (**d**) As implied in (a), the ion homeostasis model included variable axoplasmic and external volumes plus a Na/K pump and pumps leak as well as the usual HH conductances. Shaded regions labeled with **m** are myelinated. A fraction of the nodal axolemma is depicted as having incurred damage by becoming dissociated from the spectrin-actin-based cortical cytoskeleton

Table 1 Inputs to models. Axon model *without* pump (single or multi-node myelinated axon)

**Membrane capacitance	C=1 μF/cm^2
**Stimulating current	I_{stim}=12 μA/cm^2
**Transient Na conductance, maximal	g_{Na}=120 mS/cm^2
**Transient K conductance, maximal	g_K=36 mS/cm^2
Leak conductance	g_{leak}=0.25 mS/cm^2
Na reversal potential	E_{Na}=50 mV
K reversal potential	E_K=−77 mV
Resting potential	V_{rest}=−65.5 mV
Leak reversal potential	E_{leak}=−54.4 mV
# Internodal conductance per unit area	κ=0.14 mS/cm^2 (for multi-node axons)

These values also apply to Table 2, # **only for multi-node model

Hodgkin–Huxley axon models values as used by Ochab-Marcinek et al. (2009)

ohmic leak, I_{leak}. When the model specifies volumes and allows for concentration changes, currents carried by the electrogenic Na/K-ATPase (pump) are present, and leak conductances specifically for Na^+ and K^+ are included. Tables 1, 2 and 3 lists values used in the models. Model equations were solved using a 4th order Runge–Kutta scheme with variable time-step.

Table 2 Inputs to models. Single node model *with* pump

Temperature	T=293.15 K
Volume of inside compartment	vol_i=3×10^{-15} m^3 (not varied here)
Volume of outside compartment	vol_o=3×10^{-15} m^3 (varied in simulations)
Surface area	S=6×10^{-8} cm^2
Initial inside Na concentration	$[Na]_i$=20 mM
Initial outside Na concentration	$[Na]_o$=154 mM
Initial inside K concentration	$[K]_i$=150 mM
Initial outside K concentration	$[K]_o$=6 mM
Initial Na reversal potential	E_{Na}=51.5 mV
Initial K reversal potential	E_K=−81.3 mV
Intact resting potential	V_{rest}=−59.9 mV
K pump leak conductance	g_{Kleak}=0.1 mS/cm^2
Na pump leak conductance	g_{Naleak}=0.25 mS/cm^2
Leak conductance	g_{leak}=0.5 mS/cm^2
Leak reversal potential	E_{leak}=−59.9 mV
Maximum pump current	$I_{maxpump}$=90.9 μA/cm^2
Pump K- Michaelis-Menten constant	K_{mK}=3.5 mM (extracellular)
Pump Na- Michaelis-Menten constant	K_{mNa} =10 mM (intracellular)
Pump current at V_{rest}	I_{pump}=10.731 μA/cm^2

Based on values from Kager et al. (2000) and Läuger (1991)

Table 3 Inputs to models. Parameters for the Nav-CLS model of traumatic Nav-leak (for all simulations)

Fraction of affected channels	AC=0…1, as specified
Left-shift of the affected channels	LS_{AC}=0…35 mV, as specified
Coupled shifts of m and h V_m-midpoints	for AC>0 and/or LS_{AC}>0, apply Eq. (10)

See Materials and Methods

2.1 The basic axon model

Axonal voltage excursions are modeled for individual nodes of Ranvier with HH kinetics. The master equation for membrane potential V_m *(t)* at a single node is:

$$\frac{dV_m}{dt} = \frac{-1}{C}(I_{Na} + I_K + I_{leak} + I_{\text{int}} + I_{stim}), \tag{1}$$

where t is time, C is nodal membrane capacitance, I_{int} is the interaction current between adjacent nodes and I_{stim} is stimulating current, supplied as required at the first node. Currents are independent from each other except through V_{m}. I_{Na} is modeled in HH fashion as:

$$I_{Na} = m^3 h \overline{g}_{Na}(V_m - E_{Na}), \tag{2}$$

with $\overline{g}_{Na}$ the maximal conductance through Nav channels and E_{Na} the sodium reversal potential. m and h are the voltage- and time-dependent activation and inactivation variables, (i.e. m=$m(V_m,t)$ and h=$h(V_m,t)$) such that m^3h gives the open probability of a channel, and are given by:

$$\frac{dm}{dt} = \alpha_m(1-m) - \beta_m m, \tag{3}$$

$$\frac{dh}{dt} = \alpha_h(1-h) - \beta_h h, \tag{4}$$

with rate constants given by:

$$\alpha_m = 0.1\frac{(V_m+40)}{1-\exp[-(V_m+40)/10]}, \tag{5}$$

$$\beta_m = 4\exp[-(V_m+65)/18] \tag{6}$$

$$\alpha_h = 0.07\exp[-(V_m+65)/20], \tag{7}$$

$$\beta_h = \frac{1}{1+\exp[-(V_m+35)/10]}. \tag{8}$$

The units of potential and time in Eqs. (5) to (8) and throughout this work are mV and ms respectively.Eqs. (3) and (4) can be expressed in the form:

$$\frac{dx}{dt} = \frac{x_\infty - x}{\tau_x}, \tag{9}$$

where x represents the m or h variable, and with $x_\infty(V_m) = \frac{\alpha_x}{\alpha_x+\beta_x}$ and $\tau_x(V_m) = \frac{1}{\alpha_x+\beta_x}$.

2.2 Adding coupled left-shift (Nav-CLS) to axon models

To left-shift Nav channel function, i.e. to simulate effects of experimental membrane trauma on Nav1.6 (Wang et al. 2009), both functions for m and h (i.e. $x_\infty(V_m)$ and $\tau_x(V_m)$) are displaced towards more hyperpolarized potentials. This is accomplished by the simple expedient of replacing V_m in Eqs. (5) to (8) by (V_m+LS_{AC}), where LS_{AC} is the left-shift of affected channels (AC). This approach finds direct experimental justification in the behavior of Nav1.6 channels in membranes subjected to mechanical trauma, as illustrated in Fig. 2(c) (see also Fig. 3 of Wang et al. 2009). Additionally, to account for situations where some fraction of nodal channels are traumatized while the rest remain intact, the fraction of affected channels, AC, that have undergone a left-shift, LS_{AC}, of "X" mV, is included in Eq. (2) (see Fig. 1(d); ~40% of this node is blebbed: AC=0.4) and total nodal I_{Na} for the damaged node becomes:

$$I_{Na} = \left[m^3 h(1-AC) + m_{LS}^3 h_{LS} AC\right](V_m - E_{Na})\overline{g}_{Na}. \quad (10)$$

Since the only channel-related change is a voltage-shift (by LS_{AC}) of m and h functions, we term the model of trauma embodied in Eq. (10) "coupled left-shift" (CLS) (Fig. 2(a)).

Overlap of the activation and availability Boltzmanns accounts for a steady-state window conductance that underlies a voltage-dependent persistent current (Fig. 2(b)). CLS decreases window conductance near 0 mV while increasing it near a typical axonal resting potential. The now more-hyperpolarized foot of the activation curve falls too close to firing thresholds, so the left-shifted Nav channels (Nav-CLS) are "leaky" even though their steady-state current at 0 mV is reduced.

A non-inactivating I_K contributes to membrane repolarization during APs and is modeled as:

$$I_K = n^4 \overline{g}_K (V_m - E_K), \quad (11)$$

where $\overline{g}_K$ is the maximal potassium conductance and E_K is the potassium reversal potential, n^4 is the voltage-dependent open probability and evolves according to:

$$\frac{dn}{dt} = \alpha_n(1-n) - \beta_n n, \quad (12)$$

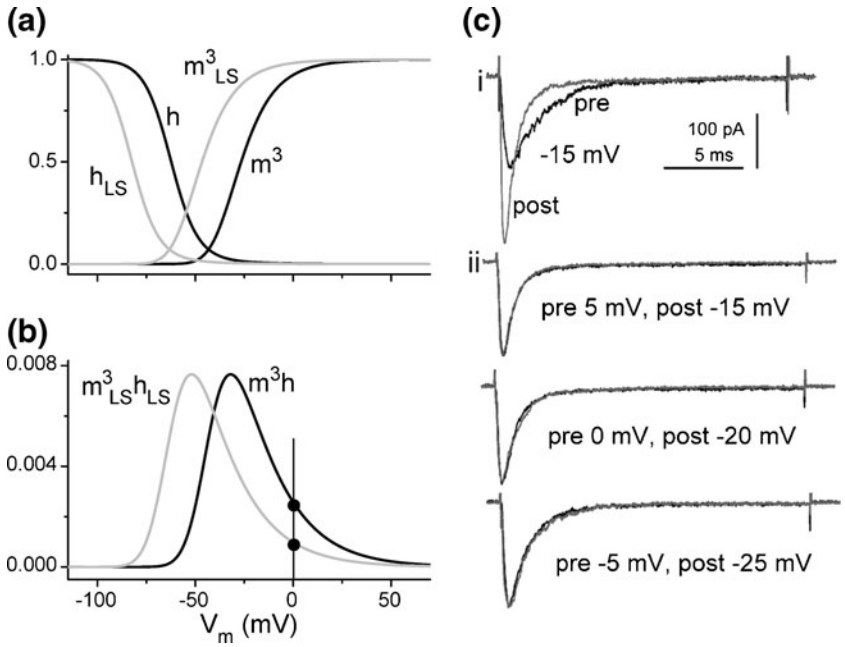

Fig. 2 Coupled left-shift (CLS) model of trauma: displaced window current as "Nav- leak". (**a**) Equilibrium values of activation ($m^3(V)$) and inactivation ($h(V)$) variables for the intact membrane (*black*) and after a 20 mV left-shift (*grey*). (**b**) The steady-state open probability, m^3h, of the intact and 20 mV left-shifted condition yields a "window conductance" whose magnitude is less at 0 mV (*vertical line and circles*) but greater at voltages nearer to normal V_{rest} (−65.5 mV in fixed concentration calculations). (**c**) Example of recombinant Nav1.6 current before (*black*) and after (*grey*) a mechanically-induced membrane damage **i)** $I_{Na}(t)$ upon stepping to −15 mV before and after traumatic stretch. **ii)** From this patch, before/after, data peak-normalized $I_{Na}(t)$, as labeled, illustrating that for this particular patch, and for this particular trauma, a coupled left-shift (i.e. "CLS") of 20 mV fully accounted for the trauma-induced kinetic (i.e., time course) changes (modified from Wang et al. (2009), where smaller and larger CLS examples are also illustrated)

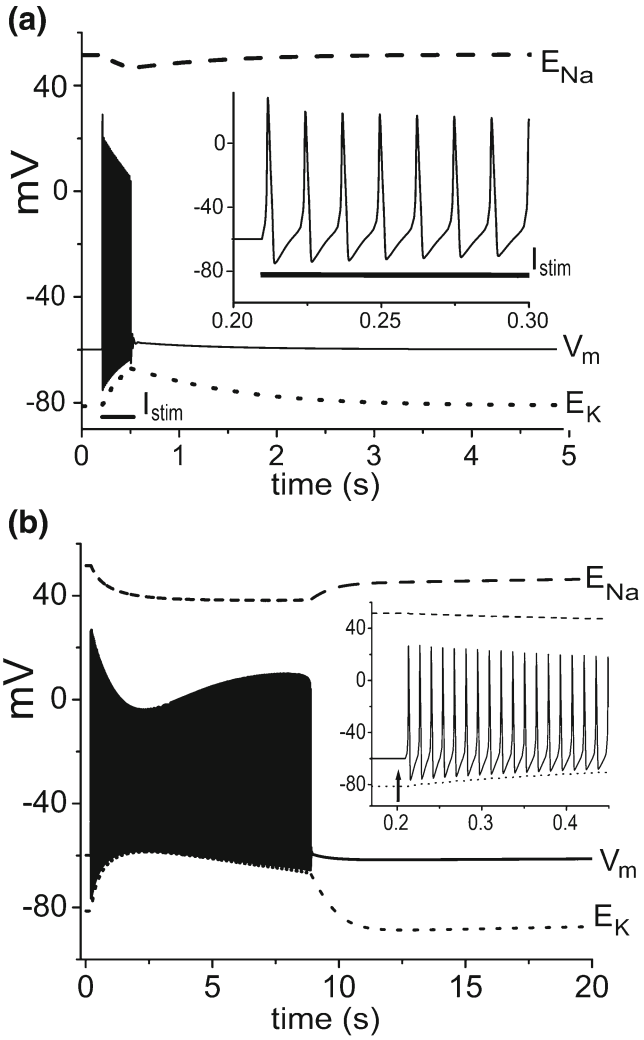

Fig. 3 Testing the full system. (**a**) I_{stim} is applied (black bar) to an intact node (AC=0, LS_{AC}=0 mV). It fires a prolonged burst, causing ion gradients to slowly dissipate (see E_K and E_{Na}). After I_{stim} is terminated, firing stops and system variables slowly return to their initial levels; this shows that the node system is computationally stable. (**b**) When a mild CLS-trauma affecting all Nav channels in the node (AC=1, LS_{AC}=1.5 mV) is imposed (see *arrow* in expanded inset), the system fires spontaneously (there is no I_{stim} here). By ~10 s, due to pump activity, the system has settled into a new slightly hyperpolarized (by 2 mV) steady-state. Note the different time scales in **A** and **B**

with:

$$\alpha_n = 0.01\frac{(V_m+55)}{1-\exp\left[-\frac{V_m+55}{10}\right]}, \tag{13}$$

$$\beta_n = 0.125\exp\left[-\frac{V_m+55}{10}\right] \tag{14}$$

I_{leak}, the leak current, is given by:

$$I_{leak} = \overline{g}_{leak}(V_m - E_{leak}). \tag{15}$$

2.3 Saltatory propagation

We use the simplest model of saltatory propagation in myelinated axons (e.g., Ochab-Marcinek et al. 2009), which assumes myelin to be a perfect insulator and each node is connected to its neighbor by a simple resistor representing the internodal axoplasmic conductance, κ, as in Fig. 1(c). We used a κ value (Table 1) shown by Ochab-Marcinek et al. (2009) to yield 1:1 node-to-node transmission of APs, which would therefore mimic the situation for typical-sized internode distances of 1–2 mm (see their Fig. 2), though note that this simplest version of saltatory propagation leaves geometries implicit. The interaction current for node i is then given by:

$$I_{\text{int}} = \kappa[V_m(i-1) + V_m(i+1) - 2V_m(i)] \tag{16}$$

at every node except the first and the last one where it is given (in a ten-node axon; Fig. 1(b)) respectively by:

$$I_{\text{int}} = \kappa[V_m(2) - V_m(1)], \tag{17}$$

$$I_{\text{int}} = \kappa[V_m(9) - V_m(10)]. \tag{18}$$

where $V_m(i)$ is the membrane potential at node i.

In the intact 10-node axon, each node faithfully (1:1) reproduces and propagates (after a brief delay for next-node capacitance charging) APs stimulated at node #1. This is true for I_{stim} or $-I_{stim}$. An "operational length constant" of this simple multi-node model can be gauged by injecting a prolonged hyperpolarizing stimulus (we used $-I_{stim}$) at node #1. This yields (at steady-state) a V_m change at node #2 that is slightly less than 1/e of the V_m change elicited at node #1. Thus, the (scale-free) length constant is slightly less than one node-to-node distance. Turn-off of—I_{stim}, we note, elicits, at node #1, a single "anode break"-induced action potential that propagates faithfully to node #10.

2.4 Modeling ion homeostasis plus excitability in an injured node of Ranvier

In this section a single injured node of Ranvier with pumps is considered without or with injected current. The basic equation for this model is:

$$\frac{dV_m}{dt} = -\frac{1}{C}\left(I_{Na} + I_K + I_{Napump} + I_{Kpump} + I_{Naleak} + I_{Kleak} + I_{leak} + I_{stim}\right), \tag{19}$$

where I_{Napump} and I_{Kpump} are Na and K currents generated by the Na/K pump and I_{Naleak} and I_{Kleak} are ohmic Na and K leaks (g_{Naleak} and g_{Kleak}) needed to provide a stable V_{rest} for the HH system when the Na/K pump is added (see Kager et al. 2000). The other currents are as previously defined.

The Na/K pump is an ATP-driven transporter that uptakes 2 K^+ and extrudes 3 Na^+ per cycle. It is weakly dependent on membrane potential and strongly dependent on the Na^+ and K^+ binding site kinetics and respective concentrations. Because the pump reverses at a very hyperpolarized potential (~−200 mV (Lemieux et al. 1992)), and is weakly dependent on membrane potential over the range studied, we use the pump current formulation given by Läuger (1991) (see also Kager et al. 2000):

$$I_{Kpump} = -2I_{\max pmp}\left(1+\frac{K_{mK}}{[K^+]_o}\right)^{-2}\times\left(1+\frac{K_{mNa}}{[Na^+]_i}\right)^{-3} \tag{20}$$

$$I_{Napump} = -\frac{3}{2}I_{Kpump} \tag{21}$$

where I_{maxpmp} is the maximal current generated by the pump and K_{mK} and K_{mNa} are Michaelis-Menten dissociation constants. The specific pump leaks for ion species X (i.e. Na^+ or K^+) are:

$$I_{Xleak} = \overline{g}_{Xleak}(V_m - E_X) \tag{22}$$

Concentrations in intracellular and extracellular compartments change as ions X flow in and out as given by:

$$\frac{d[X]_i}{dt} = -\frac{I_{XT}S}{Fvol_i}, \tag{23}$$

$$\frac{d[X]_o}{dt} = \frac{I_{XT}S}{Fvol_o} \tag{24}$$

where F is the Faraday constant, vol_i and vol_o are volumes of interior and exterior compartments respectively, S is nodal surface area and I_{XT} denotes total currents for ion species X (e.g., $I_{NaT} = I_{Na} + I_{Napump} + I_{Naleak}$).

The reversal potential of X (Na^+ or K^+) is calculated as:

$$E_X = -\frac{RT}{F}\ln\frac{[X]_i}{[X]_o}. \tag{25}$$

For the system to attain a steady-state, leak conductances and maximal pump activity need to be balanced. Since Na/K ATPase uptakes 2 K^+ per 3 Na^+ extruded, pump leak conductances are adjusted so total Na^+ and K^+ currents have a ratio of 3:2 at the initial concentrations with the resting potential at −59.9 mV. Maximal pump activity is then set to bring the system to steady-state (i.e. total currents for each ion species are zero).

The parameters used for the myelinated axon and the single node models are found in Table 1 for no-pump axons and in Table 2 with pumps included. Table 3 indicates the parameters involved in modeling "CLS trauma" (the experimental and mechanistic underpinnings of which are found in Fig. 2).

3 Results

3.1 Testing the full one node system (channels, pumps, volumes) without and with a CLS-type "trauma"

The global stability of the control system, a single intact node, with pumping included was tested with a prolonged injection of current, I_{stim}, that elicits a train of action potentials (APs) (see Fig. 3(a)) (parameter values in Tables 1 and 2). During the train, ion gradients dissipated, but when I_{stim} was stopped, pump activity was able to slowly return the system to its initial state. The system, in other words, was stable. Next, in Fig. 3(b), we show that when a mild CLS is applied (at the arrow in the insert), the node begins to fires spontaneously (i.e. with absolutely no injection of I_{stim}). The system, in other words, exhibits ectopic activity. This abnormal (spontaneous) activity continues for almost 10 s then V_m abruptly settles to a new steady state.

In simulating and monitoring trauma in this way, the intact systems (sometimes without pumps, or as here, with pumps) are allowed to reach steady-state (~100 ms) then a CLS (see Materials and Methods) is applied. Once a new steady-state is reached (100–500 ms depending on the simulation), spike counting begins (typically for 5 s). Where applicable, I_{stim} is then applied; this serves to further probe whether the system's excitability properties have changed due to the CLS. For AP trains, firing rates (spikes/s) are assessed by counting each time V_m crosses some value (typically −15 mV) in the positive direction.

3.2 Single node- fixed ion concentrations (i.e. no pumps)

The basic consequences of Nav-CLS for system excitability were examined with ion concentrations fixed (i.e., no pumps), simulating short time scales. To limit model complexity only one node is considered in this section (parameter values in Table 1). AC and LS_{AC} are systematically varied to simulate blebbing of different fractions of nodal membrane (AC) (Maxwell 1996) to different degrees of severity (LS_{AC}) (Wang et al. 2009). The computed firing rates are plotted in Fig. 4. The rates were obtained as illustrated in the sample $V_m(t)$ trajectories of Fig. 5(a), and the distinctive trajectory patterns are described and characterized as trauma behaviour regimes in the next paragraph.

Applying a relatively small CLS to a large enough fraction of Nav channels (I_{stim}=0) induces what we term "spontaneous" firing when the shifted component of window current is large enough near V_{rest} to depolarize V_m past threshold. In Fig. 5(a) the grey symbols marked "spontaneous" reproduce the *AC=1* plot of Fig. 4(c). Figure 5(a) also reproduces, overlapped, the *AC=1* plot of Fig. 4(d) which is for "stimulated" (black symbols) nodes. The regimes identified are intact and a–d: they are characterized by the combination of their spontaneous (grey bar) and stimulated (black bar) firing patterns. The traces below exemplify the patterns. Intact nodes show no spontaneous firing and respond to I_{stim} with tonic firing. In regime **a** ("hypersensitive") there is no spontaneous firing but I_{stim} elicits tonic firing at frequencies linearly increasing with LS_{AC}. In regime **b** ("tonic firing") the node shows spontaneous tonic firing and I_{stim} elicits tonic firing at even higher frequencies; both firing rates increase linearly with LS_{AC}. In regime **c** ("tonic firing/depolarizing block") the node shows spontaneous tonic firing but is in fact on the brink of inexcitability; firing is eradicated by I_{stim}, which causes a sustained depolarization and renders the axon refractory. In regime **d** ("depolarizing block") the node's response to injury is a rapidly damped burst of firing ending in a sustained depolarization; I_{stim} elicits no appreciable change, verifying that the node is inexcitable (inactivation prevails).

Following a similar analysis the entirety of Fig. 4 data is collated in Fig. 5(b) which is a trauma behavior regime diagram. This diagram shows that increases of *AC* and/or LS_{AC} will contribute to the overall severity of Nav-CLS injury. The regime plot is dominated by tonic firing, either spontaneous or stimulated. At some point however depolarizing block takes over. To visualize how varying Nav-CLS injury affects total nodal window current, we have plotted in Fig. 6 examples of some Nav window conductances. This plot also indicates some key system values along the V_m axis (e.g., $V_{rest.,}$ and $V_{0.5}$ for $n^4(V)$, which is the gating variable for Kv P_{open}). When Nav channels suffer a CLS, threshold potentials will left-shift as the activation limb of the window conductance moves leftward (Fig. 6). Exacerbating this gating-shift aspect of "Nav-leak", the driving force on the injured component of window conductance increases to (V_m+LS_{AC} -E_{Na}) instead of the intact value (V_m-E_{Na}).

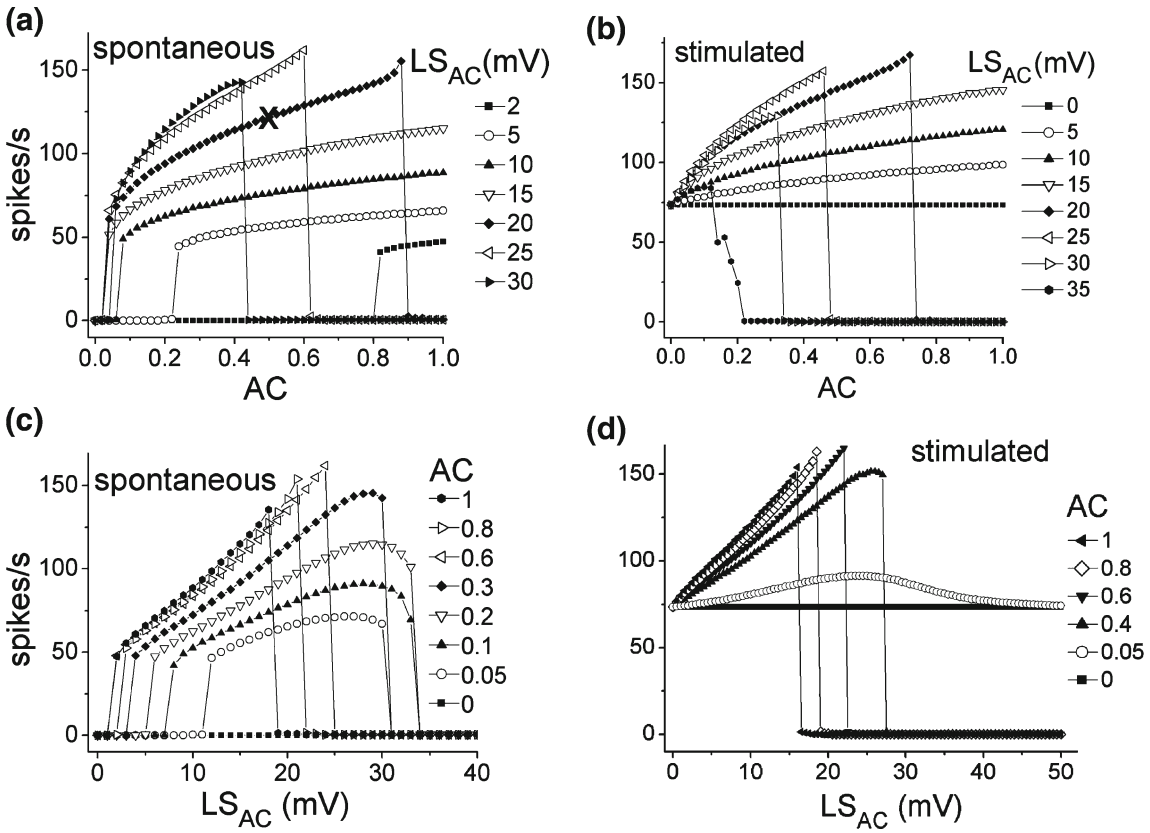

Fig. 4 CLS-induced spontaneous and stimulated firing rates in a no-pump node. Tonic firing rates as the fraction of affected channels (*AC*) and the magnitude of coupled left-shift of affected channels (LS_{AC}) is varied, without (**a**, **c**) and with stimulation (**b**, **d**). Frequencies were assessed after the initial rapidly damped voltage excursions. For stimulation, I_{stim} (Table 1) was injected once the "CLS-trauma" had been imposed and the system was at its new (post-"injury") steady-state condition. Examples of the modeled $V_m(t)$ traces used to generate these plots are shown in Fig. 5(a) (intact, *a*, *b*, *c*, *d*); note both the post-injury settling process and the subsequent response to I_{stim}. The X marked in **A** (at *AC*=0.5, LS_{AC}=20 mV) corresponds to "*AC*=0.5" in Fig. 6; the same condition is also marked with an X in Fig. 5(b)

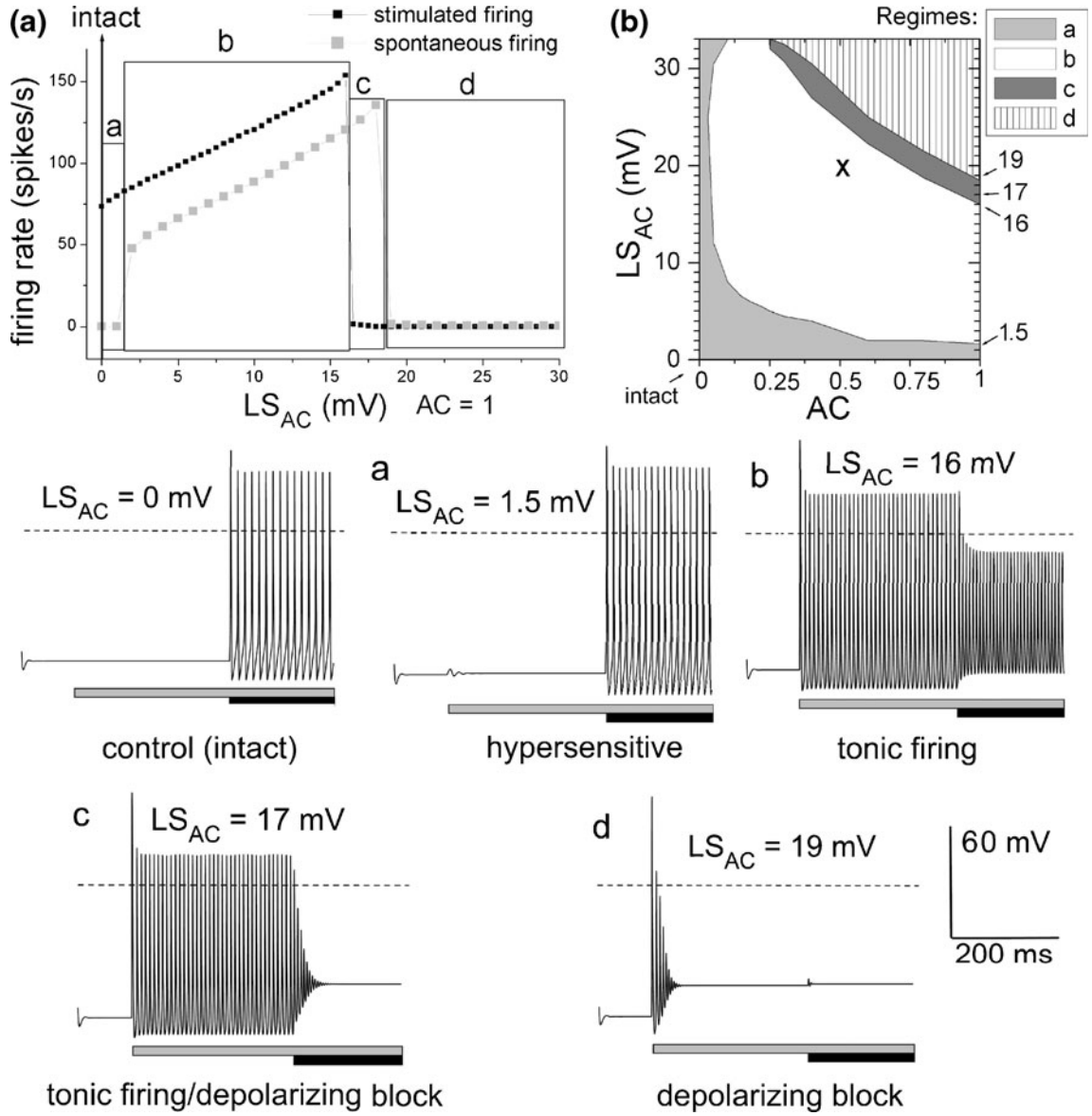

Fig. 5 Excitability regimes at a single no-pump node of Ranvier; intact and increasing CLS. (**a**) For AC=1, comparing firing rates for CLS-induced activity without (spontaneous) and with I_{stim} (stimulated) for increasing LS_{AC} (these overlapping plots are extracted from Fig. 4c,d). Below are examples of $V_m(t)$ for the **intact** situation and for four distinctive regimes of trauma-behavior: **a,** hypersensitive**; b,** tonic firing; **c,** tonic firing/depolarizing block; **d**, depolarizing block. Dashed lines indicate 0 mV. Nav-CLS (*grey bars*) imposed at 100 ms, then I_{stim} (*black bars*) at 400 ms. (**b**) For all the conditions covered in Fig. 4, activity regimes for a node are constructed according to the definitions in **A.** Note that the $V_m(t)$ examples used for **A** fall along the right hand y-axis (AC=1). The X is explained in the legend to Fig. 4

Thus CLS injury yields spontaneous tonic firing. But as injury becomes increasingly severe, decreased availability (corresponding, as indicated in Fig. 6, to the right-hand side of the window conductances) dominates over the influence of the stimulatory (CLS-enhanced) window current, and spontaneous firing is lost. For an example (AC=1) of the transition from spontaneous tonic firing to a fully refractory condition, consider Fig. 5a*c* and a*d*. There, as LS_{AC} goes from 17 mV to 19 mV, spontaneous tonic firing gives way to rapidly damping APs that culminate in a new depolarized V_{rest}. Crucially, however, even if excitability has been lost, the Nav window conductance ("Nav-leak") provides a dangerously large component of the resting conductance. In Fig. 6 with LS_{AC}=20 mV, for instance, the depolarized V_{rest} almost coincides with the peak value of the window conductance.

It is interesting to consider a seemingly mild trauma of AC=0.05, equivalent to a bleb encompassing 5% of nodal membrane. For LS_{AC}<12 mV (Fig. 4(c), open circles) spontaneous firing is absent, but above that (LS_{AC} 12 mV to

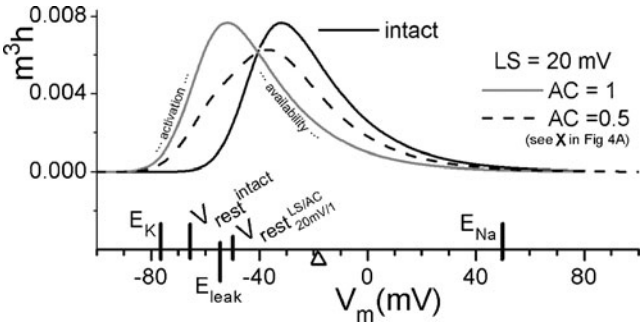

Fig. 6 Dysfunctions of excitability and coupled left-shift. Window conductances, $m^3h(V)$, for the intact system and for two variants (AC=1, AC=0.5) of a 20 mV Nav-CLS, plotted with important potential values labeled to indicate where the normal (AC=0) and damage-shifted window conductances would fall relative to system driving forces and conductance parameters. The AC=0.5 condition is highlighted in Figs. 4 and 6 with an X. Only one of the window conductances has labels on its activation-dominated and availability– i.e. inactivation- dominated limbs (left-side and right-side respectively) but this applies to all of them. The HH axon threshold voltage is ~−57 mV (a value determined from bifurcation analyses). The triangle marks −19 mV, the midpoint of n^4(V), the activation Boltzmann for HH Kv channels. The 3 situations: intact node (AC=0, LS_{AC}=0 mV), node with the entire membrane traumatized (AC=1, LS_{AC}=20 mV), node with half the membrane traumatized (AC=0.5, LS_{AC}=20 mV). For Nav1.6 channels, 20 mV represents a very large (albeit not maximal) left-shift (Wang et al. 2009). Together with Fig. 2a (equilibrium curves for h(V) and m^3(V)), these plots encapsulate how window currents are linked to nodal excitability. V_{rest} in intact nodes is well below peak m^3h(V), so no I_{window} flows unless an external stimulus depolarizes V_m. With the entire node traumatized, V_{rest} almost coincides with peak m^3h(V) and the system is inexcitable. The AC=0.5 case exemplifies a situation where a "subthreshold persistent I_{window}" triggers spontaneous tonic firing; V_{rest}, being ill-defined under these circumstances, is not plotted

30 mV) the maximal (shifted) window conductance is close enough to V_{rest} (illustrated in Fig. 6 for LS_{AC}=20 mV) that the shifted portion of window current is large enough to induce spontaneous activity. The Nav-CLS could be seen as a stimulating current "setting off" the rest of the node.

If one then considers the AC=0.05 case with an actual application of I_{stim} (Fig. 4(b,d)), it is immediately evident that the mild CLS has rendered the axon hyperexcitable, even in the LS range with no spontaneous activity. Likewise for another variant of mild trauma, i.e. small LS_{AC}, large AC (Fig. 4(b,d)). Such Nav-CLS-induced hyperexcitable responses to what would normally be a barely supraliminal stimulus could contribute to sensory allodynia such as reported for damaged "algoneurons" (Fried et al. 2011).

For large AC, spontaneous firing occurs at low LS but at some LS level, tonic firing gives way to a more depolarized quiescence and again, excitability is tested by injecting I_{stim}. In Fig. 4(b,d) we see that not only are axons rendered quiescent by large LS_{AC}, and less excitable than normal, but that inexcitability appears for lower values of LS_{AC} (in the Fig. 5(a) plot, compare regime c for spontaneous and stimulated firing frequencies). As illustrated for the case AC=1 (Fig. 4(d)), the transition is sharp: at LS=16 mV, I_{stim} makes the axon fire tonically (albeit at reduced AP amplitude (Fig. 5a*b*)) but at LS=17 mV, I_{stim} causes spontaneous tonic APs to rapidly damp out. Severe Nav-CLS trauma, in other words, pushes the axon to the verge of depolarizing block.

Thus, depending on Nav-CLS intensity and on whether the axon receives further inputs, the CLS model of trauma exhibits combinations of quiescence (which has hypersensitive and inexcitable versions), spontaneous (ectopic) activity, hyperactivity and rapidly-damping hypo-excitability.

3.3 What if gK left-shifted too?

At the node of Ranvier, g_{Na} dominates over g_K in an even more pronounced fashion than in the HH model. Nevertheless, for the sake of interest, we tested (not shown) in our HH-based model, the effect of left-shifting Kv channels to the same extent as the Nav channels (i.e., for the several CLS conditions illustrated in Fig. 5(a) *a-d* plus a few others). Thus, at trauma onset (AC=1) the conditions were, Nav-CLS/K-LS: 1.5, 5, 16, 17, 19, 24 mV). In general, these double-shifts hold off the onset of spontaneous AP trains until larger LS values (in cases of mild trauma, this could seen as "protective") but then, with deepening LS, the double-shifts yielded ectopic bursting up to more depolarized levels, albeit involving voltage oscillations of increasingly reduced amplitude (these unwanted Na^+ influxes would render the severe double-shifts even more deleterious than severe Nav-CLS alone). Traumatic left-shift of multiple conductances would likely be untidier than "equal left-shifts". At nodes of Ranvier, Nav and Kv channels are spatially separated, and along axon initial segments, too, expression of channels is spatially heterogeneous (Duflocq et al. 2011). Nav and Kv channels likely inhabit different lipid nano-environments (Gu and Gu 2011), and, given their structural and kinetic distinctiveness, would differ in their inherent specific propensities to left-shift due to bilayer disorder (Morris 2011c).

3.4 Propagation along a myelinated axon

For saltatory propagation in a simulated myelinated axon (without pumps) (Fig. 1(b,c)), the computational procedure necessarily has added features. With CLS applied at the injured mid-axon node (#6), nodes equilibrate individually for 100 ms, then internode interactions are turned on. The interconnected node system is allowed to re-equilibrate for 150 ms. AP frequency is then measured, typically for 5 s. An injured node operating in trauma activity regime **b** or **c** fires spontaneously, and these ectopically generated mid-axon APs propagate in both directions. Note the delayed

arrival of APs at node #10 in Fig. 7(a) (for a regime b injured node #6). This would send inappropriate signals towards both axon terminals and the neuronal soma.

In Fig. 7(b) a severely injured node #6 (regime **d**) exhibits a damped oscillation as it settles to its new depolarized value while nodes #1 and #10 have normal V_{rest} values. Later, with I_{stim} turned on at node #1 (black bar), node #6 blocks the APs propagating from node #1. As each **AP** propagates in from neighboring node #5 it generates in the injured node #6 only a low amplitude oscillation (see inset in Fig. 7(b)); this is consistent with the result that regime **d** nodes are inexcitable by constant I_{stim}. Similarly (but not shown in Fig. 7(b)), a regime **c** injured node, though firing spontaneously at an extremely high rate (i.e., generating ectopic excitation at node #6), blocks onward propagation of incoming AP traffic because the extra depolarizing input results in regime **c** type depolarizing block.

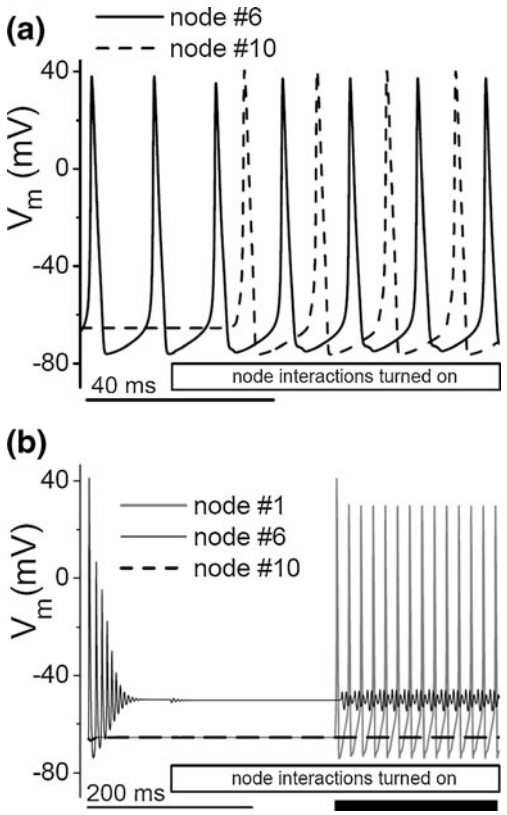

Fig. 7 Saltatory action potential propagation and CLS trauma. (**a**) $V_m(t)$ at the spontaneously firing injured (AC=1, LS_{AC}=7 mV) node #6 and at node #10. Node #1 (not shown) fires like node #10. The delay between node #6 and #10 action potentials represents the propagation time through the intervening nodes. (**b**) $V_m(t)$ at initial (#1), injured (#6) and end (#10) nodes. Injury (AC=1, LS_{AC}=19 mV) is at t= 0 ms. Node #1 stimulation (*black bar*) starts at t=300 ms. APs propagate to node #6, whose regime *d* injury blocks further propagation. Subsequent nodes (e.g. node #10) remain inactive. The inset is a blow-up of the first part of the adjacent traces

When the injured mid-axon node spontaneously fires and sends APs in both anterograde and retrograde directions (see Fig. 7(a)), not all spikes are transmitted. As firing frequency in the injured node increases with LS_{AC} (keeping $AC=1$) it eventually becomes too rapid for the uninjured adjacent nodes: consecutive injured-node APs that occur during the refractory period of adjacent nodes are not both transmitted. Thus firing frequency at the adjacent (intact) node decreases.

For axons receiving no I_{stim} at node #1, Fig. 8ai plots spike frequencies for an injured node (#6) spontaneously firing and an adjacent intact node as LS_{AC} is increased. All intact nodes fire at the same frequency since APs in intact nodes are faithfully transmitted. With increasing LS_{AC}, the system changes from propagating all ectopic APs (1:1 propagation) to propagating only 2 for every 3 generated at the injured node (3:2 propagation) to propagating only 1 for every 2 (2:1 propagation) (see Fig. 8aii). In other words, the resonant frequency of the injured node is substantially higher than that of the intact nodes.

What happens if there is incoming (anterograde) stimulation that was initated at node #1? Fig. 8(b) plots firing frequency for nodes #1, #5, #6 and #10. Node #6 is injured and, as described above, all "downstream" nodes (exemplified by 10) have exactly the same firing frequency. Node #5, however, lies between the stimulated (#1) and injured node (#6) and is impacted by the different-frequency incoming APs generated in both. Node #5 consequently shows complex erratic behavior. At nodes closer to the stimulated one (node #1), the interfering effects of the injured node are less pronounced. It should be possible to test this scenario experimentally by monitoring firing frequency at (minimally) three distant points along a myelinated axon, comparing the effect of irreversible trauma to that of reversible agents known to left-shift Nav1.6 kinetics. At the middle point, a reversible left-shifting agent could be applied e.g., highly localized heating (Thomas et al. 2009; Smit et al. 2009) then, perhaps, ciguatoxin (Hogg et al. 2002) and, finally, trauma. A change in firing frequency, or possibly a silencing of the most distal point would indicate a change in excitability mid-axon, if firing frequency behaves as modeled here. This would not only help confirm whether trauma, like heat and ciguatoxin, causes Nav channels to left-shift, but also have implications for such conditions as neuropathic pain where ectopically generated APs are the source of the condition (Devor 2009).

3.5 Ion homeostasis (one node with channels, pumps, volumes)

This section on ion homeostasis (Figs. 9, 10, 11) focuses on the consequences for Na^+-loading of Nav-CLS. We return to a single node of Ranvier, but with pumps, and thus with [Na^+] and [K^+] allowed to vary within their defined intracellular and

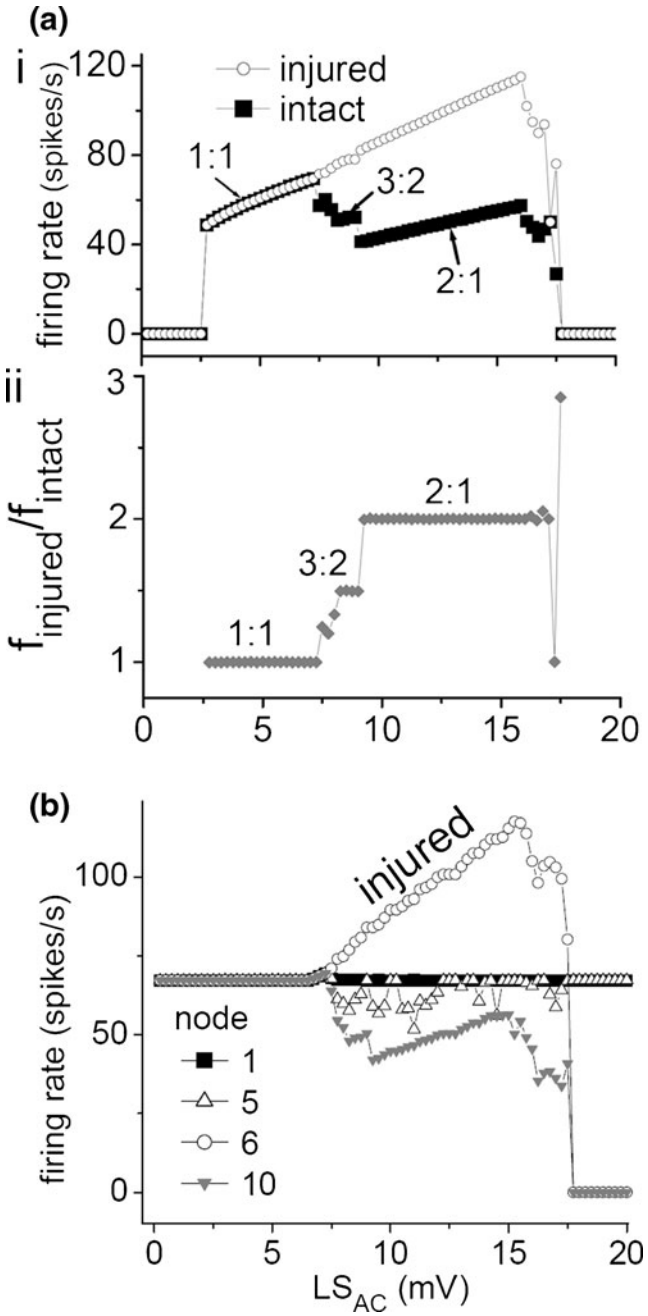

Fig. 8 Node-to-node transmission fidelity and increasing CLS trauma. (**a**) i. Spontaneous firing rate at the injured node, and triggered rates at intact nodes as LS_{AC} increases (AC=1). APs in nodes #5 or #7 propagate faithfully, so firing rates are identical in all intact nodes. However, beyond~LS_{AC}=7 mV intact nodes cannot fire as fast as the injured node. **ii.** The same data set plotted as ratios shows that as the propagation ratio diminishes with increasing LS_{AC}, it does so in integer ratios. (**b**) Firing rate at the indicated nodes when node #1 is stimulated. Nodes beyond the injured node (#6), exemplified by node #10, behave like intact nodes in (**a**), but nodes between the stimulated and injured nodes (e.g. node #5) do not, since they receive both stimulated APs propagating from node #1 and (higher frequency) ectopic APs propagating from node #6

extracellular volumes. Particulars of firing regimes identified in the previous sections can be expected to differ subtly when ion reversal potentials are free to vary. In these simulations (see Fig. 9(a)), the system was equilibrated for 200 ms then trauma was applied. As AC and LS_{AC} were varied, five different "regimes" (Fig. 9ai–v and b) were identified. The previous points regarding combination of these factors still apply: e.g., if LS_{AC} is extremely small, a large AC has negligible effect beyond hyper-excitability (*in vivo*, of course, hyper-excitability could be a decidedly non-negligible consequence). This applies, too, for small AC, large LS_{AC}. The first regime characterized (termed "transient firing") shows spontaneous firing then (over time), under the influence of pump activity, a return to a new excitable steady-state (see Fig. 9ai; not shown: excitability was verified using I_{stim}). Larger trauma induces a regime with periodic burst firing (Fig. 9aii). This is similar to responses in a comparable system (Kager et al. 2000) in which electrogenic Na/K pump current was varied: reducing a hyperpolarizing pump current there yields a similar outcome to augmenting a depolarizing current (i.e. window current) in our system. Between bursts, the membrane is excitable (i.e., I_{stim} elicits spikes, not shown). The third regime, once the system settles, consists of spontaneous tonic firing (Fig. 9aiii). The fourth (Fig. 9aiv), which we term mini-bursts, occurs for a very limited set of AC and LS_{AC} and consists of periodic bursting at a reduced amplitude accompanied by a large dissipation of the sodium gradient (i.e., from about E_{Na}=50 mV to 0 mV). Finally (Fig. 9av), major trauma renders the system inexcitable with, again, collapse of the $[Na^+]$ gradient. Interestingly, this regime, which we term "leaking-pumping" is characterized by a hyperpolarized E_K, with V_m unchanged from the control steady-state. E_K hyperpolarizes because pumps must work extra fast to compensate the very large window-current based Na^+-leak (trauma does not impair the pump in this model) and the simultaneous uptake of K^+ hyperpolarizes E_K. V_m stays unchanged because it is dominated by the unspecified leak whose reversal potential, E_{leak},, is (by definition) unaffected by the trauma-associated depletion of specific ion gradients.

3.6 ATP depletion

The Na/K pump is ATP-fuelled: as intense pumping at traumatized nodes of Ranvier depleted ATP reserves, pumps would slow or stop. As Na^+ and K^+ gradients dissipated, the Ca^{2+} gradient (coupled to Na^+ via the Na/Ca exchanger) would dissipate, triggering Ca^{2+}-mediated excitotoxicity and axon loss. These late steps are left as inferences, however, based on what we model, which is pump rates.

As depicted in Fig. 10 for 4 different values of LS_{AC} (AC=1), when Nav-CLS causes the value of E_{Na} to fall, the Na/K pumps speed up; the plots show pump current normalized to the intact steady-state rate of pumping. When E_{Na} depolarizes and E_K hyperpolarizes, pump activity, which, following Michaelis-Menten values listed in

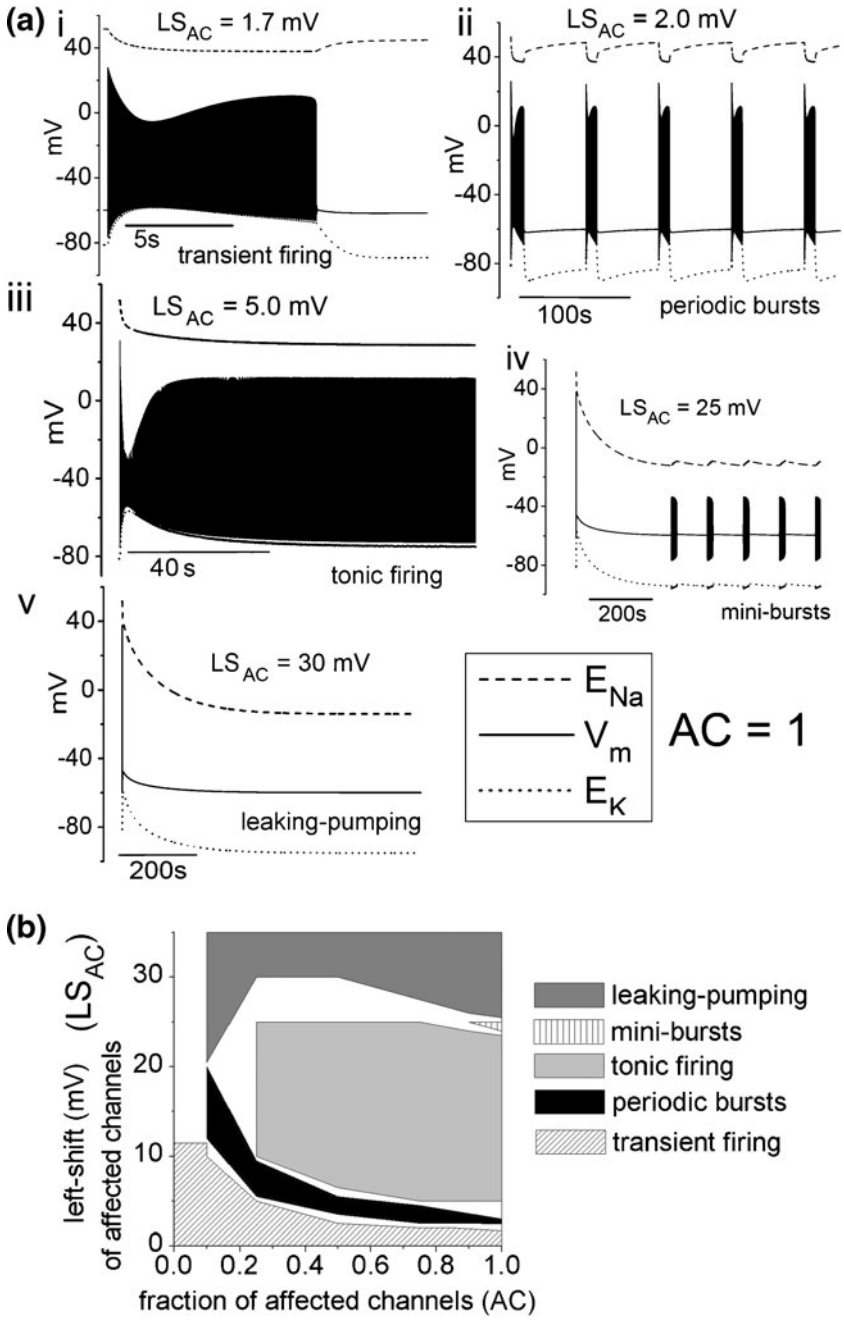

Fig. 9 (**a**) Regimes of CLS-induced activity when the pump remains active. For intact axons at steady-state, LS_{AC} is imposed at t=0. A selection of $V_m(t)$ plots (AC=1), **i** to **v** (each is also labeled with a descriptive name), are shown (note different time scales). To verify that a stable steady-state had been reached for LS_{AC}=1.7 mV, the model was run for 1,000 s. (**b**) is a summary plot of system behaviors (or "regimes", labeled with the names from (**a**) for a range of AC and LS_{AC} values. Although the regime plot is incomplete because of difficulty identifying the transitions between behaviors, it gives a qualitative picture of possible spontaneous and therefore dysfunctional (ectopic) behaviors in an axon with-Nav CLS

Table 1, is stimulated by the increasing intracellular [Na^+] and by increasing extracellular [K^+] associated with these [ion] changes. These changes can be taken as an index of ATP requirements. With a 2 mV CLS, the node fires in bursts of APs (Fig. 9ii) causing pump activity to intermittently increase 2.3-fold. A 5 mV CLS causes periodic firing and pump activity increases >2 fold in a sustained fashion. It is notable that at CLS=30 mV, even though excitability is blocked due to Nav-inavailability, E_{Na} depolarizes and E_K hyperpolarizes as a result of CLS window current based Na^+-leak; accordingly, pump activity, increases >2-fold then slowly (>5 min) decreases to an elevated steady-state that is 1.6-fold above the normal pump rate. At the other trauma extreme, even the small CLS traumas seen in Fig. 9ai (1.7 mV) and Fig. 9aii (2 mV) increase pump activity >2-fold (that for the duration of spontaneous CLS-elicited firing (a one-time increase for 10 s in the case of 9Ai, and periodically, ~10 s increases every minute in the case of 9Aii (seen in Fig. 10 for this example)). Where ATP reserves were already compromised (e.g., due to trauma-related ischemia), Nav-CLS-elicited changes in axonal excitability, both for mild and extreme CLS cases, would further deplete those reserves, thus slowing the pumps and further depolarizing nodal V_m. Not surprisingly, ectopic tonic firing (due to a

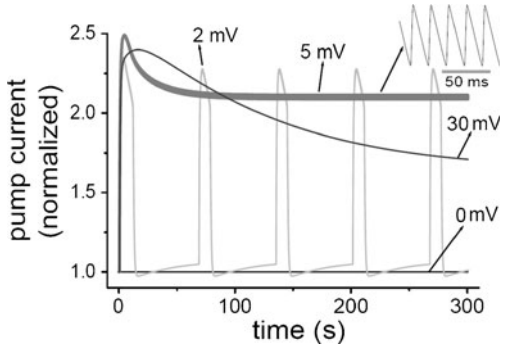

Fig. 10 Pump current, hence ATPase activity, in traumatized nodes. Pump current (normalized to the intact steady-state, "CLS=0 mV" current, which is 10.731 μA/cm^2), during 3 of the time courses shown in Fig. 9 for LS_{AC} as labeled (AC=1). For 5 mV, the broad-looking plot is actually fluctuations of pump activity as the system responds to unremitting firing

5 mV Nav-CLS; see Fig. 9aiii and Fig. 10) is the most "expensive" situation, but milder and stronger CLS situations are almost as bad in terms of ATP demands.

3.7 Changing the volume of the extracellular compartment

In the section with pumps, we have used equal-sized interior and exterior volumes, but in reality, for axons of different calibers, these compartments would vary substantially in absolute and relative terms. Moreover, both compartments' volumes could change following trauma in conjunction with blebbing, beading, osmotic swelling, edema and so on. Trauma-induced swelling of neighboring glia, accompanied by altered solute uptake capabilities and glial K-channel activity, could alter the effective volume of the exterior compartment (Kimelberg 2004; Di et al. 2000; Seifert et al. 2009). All these volume-related factors via effects on pump rates, should modulate excitability patterns, possibly yielding paroxysmal behavior patterns, as recently described for mechanistically more complex simulations by Coggan et al. (2011) and by Krishnan and Bazhenov (2011). When different volumes are considered in "with-pump" simulations, it is necessary to follow the system long enough for pump activity to bring the system to its new steady-state. Figure 11 illustrates how compartment volume can dramatically affect the patterns of (dysfunctional) excitability; for a spontaneously firing (mildly traumatized; LS_{AC}=2 mV, AC=1) node, the effect of varying exterior volume from 0.1X through to 4X the internal volume was simulated. After the CLS (the "mild trauma") was imposed at t=0, the destabilized system immediately began spiking then some time to attain a new (unstable) steady state. Although we simulated for 300 s, we have plotted only to 150 s (the systems always appeared stationary by then). Given that the underlying kinetic properties of the channels and pump were invariant (only volumes varied), the inescapable conclusion is that a wide range of concentration-dependent burst dynamics are possible as volume-and-time varying driving forces and pump currents change to cope with the systems' mildly damaged conductance mechanisms. In real systems there could be many concurrent changes in system variables, independent of the conductance mechanisms themselves: pump density and/or the maximal pump rate could change with time, unstirred layers could be a factor, external and/or internal volumes could be changing. Under those circumstances, time variant burst dynamics with characteristics "from A-to-F" (and beyond) could be anticipated, even if channel kinetics remained stable after the initial trauma-perturbation. If, with axolemmal deterioration, Nav-CLS progressively worsened (i.e. CLS >2 mV; recall that what all the patterns in Fig. 11 are for a 2 mV CLS-trauma), even a greater range of variability in burst dynamic patterns would be expected, all without invoking any novel conductance mechanisms. This mild Nav-CLS can generate subthreshold oscillations (see expanded section, Fig. 11(e)), a feature of traumatized neurons (see Kovalsky et al. 2009) as well as of neurons exposed to certain Nav toxins (Hogg et al. 2002). As Izhikevich (2001) showed, a basic HH excitability structure is sufficient to generate subthreshold oscillations like this, provided the inactivation process is dramatically slowed. Our CLS systems possess no slow inactivation process, but feature a very different slow process that develops due to pump/CLS-window-current interactions. It is self-evident that to have a chance of surviving, any mildly traumatized axon must have well-functioning pumps. Consequently, the mild Nav-CLS trauma system, as modeled here, necessarily has an emergent ultra-slow time constant, associated with Na/K pump current counteracting a "sub-threshold persistent window current-based Nav-leak".

4 Discussion

Pathologies of excitable cells are exacerbated by Nav channel dependent hyper- and/or hypo-excitability, ectopic excitation and cell loss (Mantegazza et al. 2010). Upon mechanical, ischemic, or inflammatory injuries to central and peripheral axons, Nav channels acquire elevated open probabilities. In multiple sclerosis, amyotrophic lateral sclerosis, diabetic neuropathy, epilepsy, carpal tunnel syndrome, muscular dystrophy, and more, Na^+-leak through genetically normal neuronal and muscle Nav channels impairs excitability and causes cell death (Allen et al. 2010; Kuwabara et al. 2006; Hirn et al. 2008: Weiss et al. 2010; Sun et al. 2006; Ritter et al. 2009; Misawa et al. 2009; Vucic and Kiernan 2010). For recombinant skeletal muscle and neuronal Nav channels, we previously showed that bleb-inducing membrane damage causes progressive hyperpolarizing ("left") shifts (up to ~35–40 mV) (Tabarean et al. 1999; Wang et al. 2009). Fast inactivation of Nav channels, though inherently voltage-independent, is kinetically limited by (hence,

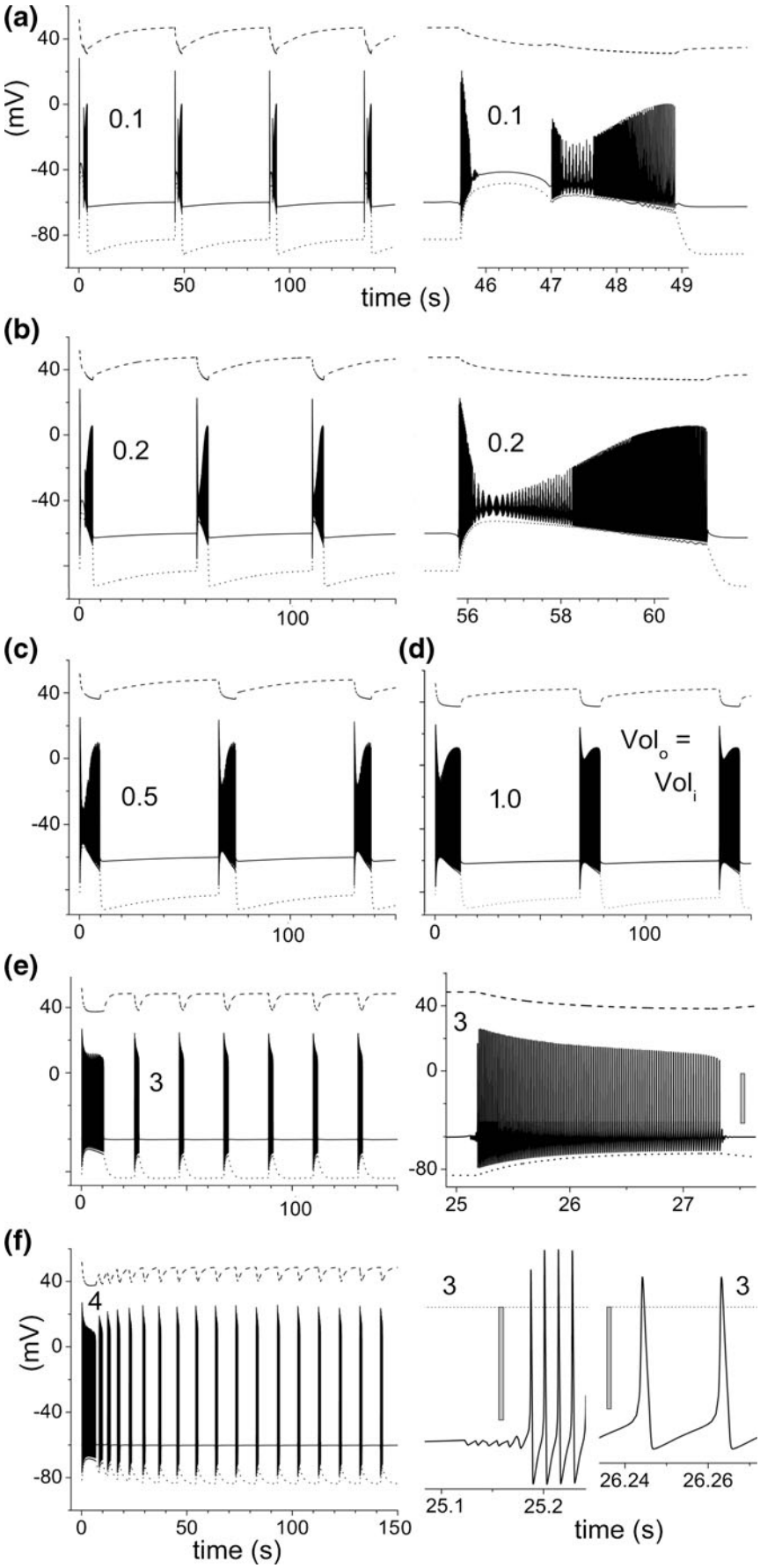

Fig. 11 System dynamics are volume-sensitive, reflecting limited pump capacity. In these simulations the entire node was given a mild CLS trauma (AC=1, LS_{AC}=2 mV) at $t=0$, which caused repetitive bursts of APs, with the ion gradients (*dashed lines* for E_{Na}, dots for E_K) varying according to the attendant Na^+ and K^+ fluxes. Going from (**a**–**f**), the relative size of the extracellular space increases: interior volume (see Tables 1 and 2) was fixed and exterior volume was varied (as labeled) as a fraction of the interior volume. Burst frequency, duration and complexity varied over a wide range. For (**a**), (**b**) and (**e**), portions of the simulations are expanded at right. For **e** (vertical grey scales: 50 mV), two parts are further expanded below (with V_m=0 mV indicated by *faint line*) to show that subthreshold voltage oscillations lead into the burst, and to show the AP shape.

coupled to) voltage-dependent activation (see Banderali et al. 2010). Thus, when activation left-shifts with membrane damage, steady-state inactivation (= availability) shifts by the same amount (Fig. 2); because of this coupled left-shift (CLS), trauma-induced changes in Nav1.6 current time courses affect the onset and decay phases to the same extent (Wang et al. 2009). Here, in light of this behavior (i.e. injury-induced Nav-CLS) of recombinant Nav channels, we investigated, for computational axons, two aspects of excitable cell physiology—Na^+/K^+ homoeostasis and excitability.

In traumatized CNS axons, nodes of Ranvier exhibit blebs that can occupy only part of a node (Maxwell 1996) and more generally, it is reasonable that bilayer damage (and hence Nav-CLS) would be of non-uniform intensity, even if it was less evident than are axon blebs or beading. Thus, for computational axons, we varied both g_{Na} left-shift intensity (LS_{AC}=0–35 mV, sometimes more) and/or the fraction of nodal axolemma affected (AC=0–1). The attendant window current left-shifts (see Fig. 5), in effect, constituted a variable damage-induced "subthreshold persistent I_{Na}".

For combined LS_{AC} and AC in the low range, the traumatized (sub)populations of Nav channels behaved like ectopic pacemaker channels, yielding tonic or burst firing of varying complexities (e.g., Figs. 5(a)*b* or 9aii). For combined LS_{AC} and AC in the high range (e.g., Figs. 5(a)*d* or 9av), effects of inactivation became dominant, so Nav-CLS blocked the axon's ability to generate APs, even in response to stimuli. Damage responses are summarized in trauma regime plots, Figs. 5(b) and 9(b) (for simulations without and with pump activity, respectively). Invariably, imposing a Nav-CLS increased Na/K ATPase activity (illustrated for small and large CLS, Fig. 10) to counteract the Na^+-loading. Secondarily, this would counter the onset of Ca^{2+}-excitoxicity. However, it is important to stress that CLS-induced "hypo-excitability" does not confer neuroprotection; the CLS large enough to render nodes inexcitable yields a strongly shifted I_{window} that continually runs down the value of E_{Na} (e.g. Fig. 9(v)).

The Na^+-loading rates and firing pattern regimes of axons with Nav-CLS depended not only on Nav gating characteristics and but also on levels of pump activity, and these in turn depended on the magnitudes of simulated axoplasmic/extracellular spaces. Conditions consistent with degeneration developed within minutes of imposing Nav-CLS (e.g. Figs. 9, 10). However, given even smaller CLSs, larger effective extracellular volumes (Huff et al. 2011), hyperpolarization-inducing contributions from K^+-channels (C. Gu and Y. Gu 2011) whose activity increased with adverse conditions (Shi and Sun 2011), and other factors, lethal Na^+-loading could plausibly be circumvented for hours or days. For mildly traumatized axons, staunching the Nav leak pharmacologically during that time window might allow for cell-mediated removal/repair of the damaged Nav-bearing axolemma, though little is known about remodeling at the mature node of Ranvier.

Myelinated tracts of the upper midbrain carry consciousness-sustaining AP traffic (Blyth and Bazarian 2010; Massimini et al. 2009). When punches accelerate/decelerate brain tissue, the midbrain incurs the highest strains and strain-rates (Viano et al. 2005); how a hook punch (e.g.) can induce almost instantaneous unconsciousness is unknown, but knockout punches constitute traumatic brain injury linked to diffuse axonal injury. If midbrain strains in cortico-thalamic tract axons abruptly caused Nav-CLS, LS_{AC}/AC magnitudes would surely differ among axons, with expected effects on AP traffic ranging from immediate onset of ectopic activity to immediate block of saltatory propagation. In some instances, the sudden multi-axon perturbation of AP traffic might suffice to ablate consciousness.

Hyperstimulating rat CA1 hippocampal neurons with epileptic discharge causes them to develop a left-shifted and enlarged Nav window current (Sun et al. 2006). In brains subjected to oxygen-glucose deprivation, the Nav-rich axon initial segments of cortical neurons are highly vulnerable to TTX-sensitive excitotoxic degeneration (Schafer et al. 2009). In all these scenarios, bilayer damage-induced CLS (secondary to ATP-deprived Na/K pumps to ATP-deprived phospholipid flippases, to reactive oxygen species build-up) could explain the Nav channel malfunctions.

Our results suggest that transient I_{Na} (in the form of displaced window current) could explain the lethal TTX-sensitive Na^+-leak of traumatized axons without invoking novel trauma-induced non-inactivating states. We do not intend to imply that Nav channels gating in slow mode(s) is irrelevant, but rather that Nav channels gating in fast mode is relevant to Nav-leak, and hence to the pharmacology of Nav-leak, in ways that may have been overlooked. In any case, slowly-inactivating Nav1.6-I_{Na}, when present, also left-shifts with membrane damage (Wang et al. 2009; Morris et al. 2012).

To model Nav-CLS-based trauma, we modified HH-type g_{Na} so it mimicked voltage clamp currents (Wang et al. 2009) in which blebbing damage and hyperpolarization altered $I_{Na}(t)$ identically (after amplitude normalization). For CLS, we applied identical AC and LS_{AC} values to the HH m and h parameters, then, for total axonal I_{Na}, summed intact and shifted populations (see Eq. (10) and the lead-up to it). The outcome was remarkably similar to the pacemaking somatic I_{Na} of rhythmically firing interneurons (Taddese and Bean 2002). For axons, of course, pacemaking type excitability is profoundly pathological. A noteable exception is the first post-soma nodes of certain neurons, where a subthreshold persistent I_{Na} facilitates high frequency firing (Kole 2011).

Hodgkin (1948) noted that over time, isolated axons generate several distinctive firing patterns and Morris and Lecar (1981) noted comparable qualitatively different firing patterns in internally-perfused giant muscle fibers. Isolated axons and cytoplasm-free muscle cells have deteriorating membranes, yet activity patterns in these "sick cells" have helped

categorize the distinctive rhythmicities of physiologically robust interneurons (Prescott et al. 2008). Evidently, physiological and pathological rhythmicities are close kin, a theme that re-emerges here (see also Coggan et al. 2010; 2011; Volman et al. 2011). Since voltage sensor stability depends on the bilayer's mechanical state (Schmidt and MacKinnon 2008; Krepkiy et al. 2009; Finol-Urdaneta et al. 2010), altering axonal bilayer intentionally (developmentally, physiologically, pharmacologically (Prescott et al. 2008; Börjesson et al. 2010)) or through misadventure (trauma, ischemia, inflammation, lipophilic poisons), will modulate neuronal excitability. It will be important to establish experimentally whether firing patterns are pushed into different regimes via bilayer-state mediated Nav (and/or Kv) shifts. The elevated lipid order characteristic of healthy Nav-rich axon initial segments may help minimize CLS (and hence spontaneous-firing). Neuroprotective Nav reagents, including omega fatty acids, are lipophilic (Li et al. 2009; Bruno et al. 2007; Bailes and Mills 2010; Isose et al. 2010) and some might partition preferentially into blebbed axolemma, giving them heightened efficacy on left-shifted channels (see Morris 2011a, b; Morris et al. 2012).

Though Nav channels strongly dominate nodal conductances, modeling trauma solely via effects on Nav channels is a clear oversimplification. Kv channels could also become left-shifted. We modeled several such conditions and found that for mild Nav-CLS/Kv-LS, co-shifting Kv is protective, while large co-shifts broaden the range over which Nav-CLS yields ectopic AP trains.

For Nav-CLS simulations with pumps, we thought it unlikely that aqueous compartment volumes would be invariant in trauma situations, and so we considered how altering the demands on pump activity would affect Nav-CLS induced ectopic bursting patterns. The consequences of the finite capacity of the Na/K pump was dramatically apparent. In a mildly traumatized system receiving assorted noisy inputs, it is reasonable to predict that irregular "paroxysms" of excitability should result. Since neurons in brain slice experiments show left-shifted Nav availability and activation due to epileptic-discharge (Sun et al. 2006) some paroxysmal behaviors seen in conjunction with epilepsy (see Coggan et al. 2011) might be explained this way.

Like Nav channels, K channels and Na/K-ATPase function is sensitive to the state of membrane lipids (Marques and Guerri 1988; Schmidt and Mackinnon 2008). Trauma inhibits Na/K pumps (Ross and Soltesz 2000), facilitates activation of background K-channels (Wan et al. 1999) and, tellingly, elicits aberrant paranodal Kv current (Shi and Sun 2011). Though Kv inhibitors helped restore propagation through traumatized nodes, the longer term reality is that any trauma-shifted Nav window current would continue to stress the pumps. A deeper understanding of the electrical and ionic dynamics of injured excitable systems can be gained from dynamical analyses (bistability and bifurcations) of the systems in question (Volman et al. (2011), Coggan et al. (2011), and Krishnan and Bazhenov (2011)). In a companion study, we have undertaken such analyses for Nav-CLS-based axolemmal damage (unpublished results, Na Yu, C.E.M, P-A. B., B.J., André Longtin). Wang et al. (2009) pointed out that traumatic damage intensity, *in vivo*, would almost certainly be "smeared out" over a range of left-shifted voltages. Some of the Nav-CLS modeling done in connection with those dynamical analyses takes that into account; here we always assumed 1or 2 subpopulations of Nav channels (AC=0 or AC=1 for one population, AC=some intermediate value for 2 populations). Smeared CLS yields a robust tendency for the behavior observed here in Fig. 11e, in which burst activity grow from and terminates with subthreshold voltage oscillations such as are a characteristic feature of neuropathic discharge (see Kovalsky et al. 2009).

In conclusion, modeling here supports the following hypothesis: the propensity of Nav channel operation to left-shift (Nav-CLS) in regions of plasma membrane bilayer damage could account for the treacherous "persistent I_{Na}" of mildly traumatized (or otherwise damaged) Nav-rich neurons. If this is correct, then window-current-based persistent I_{Na}-leak contributes to the TTX-sensitive Na^+-leaks of sick excitable cells (Morris et al. 2012). Slow-inactivated I_{Na}-leak (see Wang et al. 2009; Lenkey et al. 2011) is another possible component, but was not studied here. Ideal neuroprotective Nav-antagonists might, therefore be lipophilic molecules (Lenkey et al. 2011) whose molecular features allow them to accumulate preferentially in damaged-bilayer regions of excitable cell plasma membranes (Morris 2011b).

Acknowledgements We thank André Longtin and Na Yu for helpful discussions during the preparation of this manuscript. Our research was supported by funds from NSERC, HSF and CIHR.

References

Allen, D. G., Zhang, B. T., & Whitehead, N. P. (2010). Stretch-induced membrane damage in muscle: comparison of wild-type and mdx mice. *Advances in Experimental Medicine and Biology, 682*, 297–313.

Bailes, J. E., & Mills, J. D. (2010). Docosahexaenoic acid (DHA) reduces traumatic axonal injury in a rodent dead injury model. *Journal of Neurotrauma, 27*, 1617–1624.

Banderali, U., Juranka, P. F., Clark, R. B., Giles, W. R., & Morris, C. E. (2010). Impaired stretch modulation in potentially lethal cardiac sodium channel mutants. *Channels (Austin, Texas), 4*, 12–21.

Beyder, A., Rae, J. L., Bernard, C., Strege, P. R., Sachs, F., & Farrugia, G. (2010). Mechanosensitivity of Nav1.5, a voltage-sensitive sodium channel. *The Journal of Physiology, 588*, 4969–4985.

Blyth, B. J., & Bazarian, J. J. (2010). Traumatic alterations in consciousness: traumatic brain injury. *Emergency Medicine Clinics of North America, 28*, 571–594.

Börjesson, S. I., Parkkari, T., Hammarström, S., & Elinder, F. (2010). Electrostatic tuning of cellular excitability. *Biophysical Journal, 98*, 396–403.

Bostock, H., & Rothwell, J. C. (1997). Latent addition in motor and sensory fibres of human peripheral nerve. *The Journal of Physiology, 498*, 277–294.

Bruno, M. J., Koeppe, R. E., & Andersen, O. S. (2007). Docosahexaenoic acid alters bilayer elastic properties. *Proceedings of the National Academy of Sciences of the United States of America, 104*, 9638–9643.

Burbidge, S. A., Dale, T. J., Powell, A. J., Whitaker, W. R., Xie, X. M., Romanos, M. A., & Clare, J. J. (2002). Molecular cloning, distribution and functional analysis of the NaV1.6. Voltage-gated sodium channel from human brain. *Molecular Brain Research, 103*, 80–90.

Charras, G., & Paluch, E. (2008). Blebs lead the way: how to migrate without lamellipodia. *Nature Reviews Molecular Cell Biology, 9*, 730–736.

Coggan, J. S., Prescott, S. A., Bartol, T. M., & Sejnowski, T. J. (2010). Imbalance of ionic conductances contributes to diverse symptoms of demyelination. *Proceedings of the National Academy of Sciences of the United States of America, 107*, 20602–20609.

Coggan, J. S., Ocker, G. K., Sejnowski, T. J., & Prescott, S. A. (2011). Explaining pathological changes in axonal excitability through dynamical analysis of conductance-based models. *Journal of Neural Engineering, 8*, 065002.

Devor, M. (2009). Ectopic discharge in Aβ afferents as a source of neuropathic pain. *Experimental Brain Research, 196*, 115–128.

Di, X., Goforth, P. B., Bullock, R., Ellis, E., & Satin, L. (2000). Mechanical injury alters volume activated ion channels in cortical astrocytes. *Acta Neurochirurgica. Supplement, 76*, 379–383.

Draeger, A., Monastyrskaya, K., & Babiychuk, E. B. (2011). Plasma membrane repair and cellular damage control: the annexin survival kit. *Biochemical Pharmacology, 81*, 703–712.

Duflocq, A., Chareyre, F., Giovannini, M., Couraud, F., & Davenne, M. (2011). Characterization of the axon initial segment (AIS) of motor neurons and identification of a para-AIS and a juxtapara-AIS, organized by protein 4.1B. *BMC Biology, 9*, 66–84.

Finol-Urdaneta, R. K., McArthur, J. R., Juranka, P. F., French, R. J., & Morris, C. E. (2010). Modulation of KvAP unitary conductance and gating by 1-alkanols and other surface active agents. *Biophysical Journal, 98*, 762–772.

Fried, K., Sessle, B. J., & Devor, M. (2011). The paradox of pain from tooth pulp: Low-threshold "algoneurons"? *Pain, 152*, 2685–2689.

Gu, C., & Gu, Y. (2011). Clustering and activity tuning of Kv1 channels in myelinated hippocampal axons. *Journal of Biological Chemistry, 286*, 25835–25847.

Hirn, C., Shapovalov, G., Petermann, O., Roulet, E., & Ruegg, U. T. (2008). Nav1.4 deregulation in dystrophic skeletal muscle leads to Na^+ overload and enhanced cell death. *Journal of General Physiology, 132*, 199–208.

Hodgkin, A. L. (1948). The local electric changes associated with repetitive action in a non-medullated axon. *The Journal of Physiology, 107*, 165–181.

Hodgkin, A. L., & Huxley, A. F. (1952). A quantitative description of membrane current and its application to conduction and excitation in nerve. *The Journal of Physiology, 117*, 500–544.

Hogg, R. R., Lewis, R. J., & Adams, D. J. (2002). Ciguatoxin-induced oscillations in membrane potential and firing in rat parasympathetic neurons. *European Journal of Neuroscience, 16*, 242–248.

Huff, T. B., Shi, Y., Sun, W., Wu, W., Shi, R., & Cheng, J. X. (2011). Real-time CARS imaging reveals a calpain-dependent pathway for paranodal myelin retraction during high-frequency stimulation. *PLoS One, 6*(3), e17176.

Isose, S., Misawa, S., Sakurai, K., Kanai, K., Shibuya, K., Sekiguchi, Y., Nasu, S., Noto, Y., Fujimaki, Y., Yokote, K., & Kuwabara, S. (2010). Mexiletine suppresses nodal persistent sodium currents in sensory axons of patients with neuropathic pain. *Clinical Neurophysiology, 121*, 719–724.

Izhikevich, E. M. (2001). Resonate-and-fire neurons. *Neural Network, 14*, 883–894.

Kager, H., Wadman, W. J., & Somjen, G. (2000). Simulated seizures and spreading depression in a neuron model incorporating interstitial space and ion concentrations. *Journal of Neurophysiology, 84*, 495–512.

Kimelberg, H. K. (2004). Volume activated anion channel and astrocytic cellular edema in traumatic brain injury and stroke. *Advances in Experimental Medicine and Biology, 559*, 157–167.

Kole, M. H. (2011). First node of Ranvier facilitates high-frequency burst encoding. *Neuron, 71*, 671–682.

Kovalsky, Y., Amir, R., & Devor, M. (2009). Simulation in sensory neurons reveals a key role for delayed Na^+ current in subthreshold oscillations and ectopic discharge: implications for neuropathic pain. *Journal of Neurophysiology, 102*, 1430–1442.

Krepkiy, D., Mihailescu, M., Freites, J. A., Schow, E., Worcester, D., Gawrisch, K., Tobias, D. J., White, S. H., & Swartz, K. (2009). Structure and hydration of membranes embedded with voltage-sensing domains. *Nature, 462*, 473–479.

Krishnan, G. P., & Bazhenov, M. (2011). Ionic dynamics mediate spontaneous termination of seizures and postictal depression state. *Journal of Neuroscience, 31*, 8870–8882.

Kuwabara, S., Misawa, S., Tamura, N., Nakata, M., Kanai, K., Sawai, S., Ogawara, K., & Hattori, T. (2006). Latent addition in human motor and sensory axons: different site-dependent changes across the carpal tunnel related to persistent Na^+ currents. *Clinical Neurophysiology, 117*, 810–814.

Läuger, P. (1991). *Electrogenic ion pumps*. Distinguished lecture series of the Society of General Physiologists. Vol. 5. Sinauer Assoc., Sunderland (Mass).

Lemieux, D. R., Roberge, F. A., & Joly, D. (1992). Modeling the dynamic features of the electrogenic Na, K pump of cardiac cells. *Journal of Theoretical Biology, 154*, 335–338.

Lenkey, N., Karoly, R., Epresi, N., Vizi, E., & Mike, A. (2011). Binding of sodium channel inhibitors to hyperpolarized and depolarized conformations of the channel. *Neuropharmacology, 60*, 191–200.

Li, G. R., Sun, H. Y., Zhang, X. H., Cheng, L. C., Chiu, S. W., Tse, H. F., & Lau, C. P. (2009). Omega-3 polyunsaturated fatty acids inhibit transient outward and ultrarapid delayed rectifier K^+ currents and Na^+ current in human atrial myocytes. *Cardiovascular Research, 81*, 286–293.

Lorincz, A., & Nusser, Z. (2010). Molecular identity of dendritic voltage-gated sodium channels. *Science, 328*, 906–909.

Mantegazza, M., Curia, G., Biagini, G., Ragsdale, D. S., & Avoli, M. (2010). Voltage-gated sodium channels as therapeutic targets in epilepsy and other neurological disorders. *Lancet Neurology, 9*, 413–424.

Marques, A., & Guerri, C. (1988). Effects of ethanol on rat brain (Na+K) ATPase from native and delipidized membranes. *Biochemical Pharmacology, 15*, 601–606.

Massimini, M., Boly, M., Casali, A., Rosanova, M., & Tononi, G. (2009). A perturbational approach for evaluating the brain's capacity for consciousness. *Progress in Brain Research, 177*, 201–214.

Maxwell, W. L. (1996). Histopathological changes at central nodes of Ranvier after stretch-injury. *Microscopy Research and Technique, 34*, 522–535.

McGinn, M. J., Kelley, B. J., Akinyi, L., Oli, M. W., Liu, M. C., Hayes, R. L., Wang, K. K. W., & Povlishock, J. T. (2009). Biochemical, structural, and biomarker evidence for calpain-mediated cytoskeletal change after diffuse brain injury uncomplicated by contusion. *Journal of Neuropathology and Experimental Neurology, 68*, 241–249.

Misawa, S., Sakurai, K., Shibuya, K., Isose, S., Kanai, K., Ogino, J., Ishikawa, K., & Kuwabara, S. (2009). Neuropathic pain is associated with increased nodal persistent Na^+ currents in human

diabetic neuropathy. *Journal of the Peripheral Nervous System, 14*, 279–284.

Monnerie, H., Tang-Schomer, M. D., Iwata, A., Smith, D. H., Kim, H. A., & Le Roux, P. D. (2010). Dendritic alterations after dynamic axonal stretch injury *in vitro*. *Experimental Neurology, 224*, 415–423.

Morris, C. E. (2011a). Why are so many ion channels mechanosensitive. In N. Sperelakis (Ed.), *Cell physiology source book* (pp. 493–505), 4th Edition. Elsevier.

Morris, C. E. (2011b). Voltage-gated channel mechanosensitivity. Fact or friction? *Frontiers in Physiology, 2*, 25.

Morris, C. E. (2011c). Pacemaker, potassium, calcium, sodium: stretch modulation of the voltage-gated channels. In P. Kohl, F. Sachs, M. R. Franz, editors. *Cardiac mechano-electric coupling and arrhythmias* (pp. 42–49), 2nd Edition. Oxford University Press.

Morris, C., & Lecar, H. (1981). Voltage oscillations in the barnacle giant muscle fiber. *Biophysical Journal, 35*, 193–213.

Morris, C. E., Boucher, P-A., Joós, B. (2012). Left-shifted Nav channels in trauma-damaged bilayer: primary targets for neuroprotective Nav antagonists? *Frontiers in Pharmacology 3*, 19.

Ochab-Marcinek, A., Schmid, G., Goychuk, I., & Hänggi, P. (2009). Noise-assisted spike propagation in myelinated neurons. *Physical Review E, 79*, 11904.

Prescott, S. A., De Koninck, Y., & Sejnowski, T. J. (2008). Biophysical basis for three distinct dynamical mechanisms of initiation. *PLoS Computational Biology, 4*, e1000198.

Ritter, A. M., Martin, W. J., & Thorneloe, K. S. (2009). The voltage-gated sodium channel Nav1.9 is required for inflammation-based urinary bladder dysfunction. *Neuroscience Letters, 452*, 28–32.

Ross, S. T., & Soltesz, I. (2000). Selective depolarization of interneurons in the early posttraumatic dentate gyrus: involvement of the Na(+)/K(+)-ATPase. *Journal of Neurophysiology, 83*, 2916–2930.

Schafer, D. S., Jha, S., Liu, F., Akella, T., McCullough, L. D., & Rasband, M. N. (2009). Disruption of the axon initial segment cytoskeleton is a new mechanism for neuronal injury. *Journal of Neuroscience, 29*, 13242–13254.

Schmidt, D., & MacKinnon, R. (2008). Voltage-dependent K^+ channel gating and voltage sensor toxin sensitivity depend on the mechanical state of the lipid membrane. *Proceedings of the National Academy of Sciences of the United States of America, 105*, 19276–19281.

Seifert, G., Huttmann, K., Binder, D. K., Hartmann, C., Wyczynski, A., Neusch, C., & Steinhauser, C. (2009). Analysis of astroglial K^+ channel expression in the developing hippocampus reveals a predominant role of the Kir4.1 subunit. *Journal of Neuroscience, 29*, 7474–7488.

Shi, R., & Sun, W. (2011). Potassium channel blockers as an effective treatment to restore impulse conduction in injured axons. *Neuroscience Bulletin, 27*, 36–44.

Smith, D. H., Meaney, D. F., & Shull, W. H. (2003). Diffuse axonal injury in head trauma. *The Journal of Head Trauma Rehabilitation, 18*, 307–316.

Smit, J. E., Hanekom, T., & Hanekom, J. J. (2009). Modelled temperature-dependent excitability behaviour of a single Ranvier node for a human peripheral sensory nerve fibre. *Biological Cybernetics, 100*, 49–58.

Stys, P. K. (2004). White matter injury mechanisms. *Current Molecular Medicine, 4*, 113–130.

Stys, P. K., Sontheimer, H., Ransom, B. R., & Waxman, S. G. (1993). Noninactivating, tetrodotoxin-sensitive Na^+ conductance in rat optic nerve axons. *Proceedings of the National Academy of Sciences of the United States of America, 90*, 6976–6980.

Sun, G. C., Werkman, T. R., & Wadman, W. J. (2006). Kinetic changes and modulation by carbamazepine on voltage-gated sodium channels in rat CA1 neurons after epilepsy. *Acta Pharmacologica Sinica, 27*, 1537–1546.

Tabarean, I. V., Juranka, P., & Morris, C. E. (1999). Membrane stretch affects gating modes of a skeletal muscle sodium channel. *Biophysical Journal, 77*, 758–774.

Taddese, A., & Bean, B. P. (2002). Subthreshold sodium current from rapidly inactivating sodium channels drives spontaneous firing of tuberomammillary neurons. *Neuron, 33*, 587–600.

Thomas, E. A., Hawkins, R. J., Richards, K. L., Xu, R., Gazina, E. V., & Petrou, S. (2009). Heat opens axon initial segment sodium channels: a febrile seizure mechanism? *Annals of Neurology, 66*, 219–226.

Tokuno, H. A., Kocsis, J. D., & Waxman, S. G. (2003). Noninactivating, tetrodotoxin sensitive Na^+ conductance in peripheral axons. *Muscle & Nerve, 28*, 212–217.

Viano, D. C., Casson, I. R., Pellman, E. J., Bir, C. A., Zhang, L., Sherman, D. C., & Boitano, M. A. (2005). Concussion in professional football: comparison with boxing head impacts–part 10. *Neurosurgery, 57*, 1154–1172.

Volman, V., Bazhenov, M., & Sejnowski, T. J. (2011). Pattern of trauma determines the threshold for epileptic activity in a model of cortical deafferentation. *Proceedings of the National Academy of Sciences of the United States of America, 108*, 15402–15407.

Vucic, S., & Kiernan, M. C. (2010). Upregulation of persistent sodium conductances in familial ALS. *Journal of Neurology, Neurosurgery, and Psychiatry, 81*, 222–227.

Wan, X., Juranka, P., & Morris, C. E. (1999). Activation of mechanosensitive currents in traumatized membrane. *American Journal of Physiology, 276*, C318–C327.

Wang, J. A., Lin, W., Morris, T., Banderali, U., Juranka, P. F., & Morris, C. E. (2009). Membrane trauma and Na^+ leak from Nav1.6 channels. *American Journal of Physiology Cell Physiology, 297*, C823–C834.

Weiss, S., Benoist, D., White, E., Teng, W., & Saint, D. A. (2010). Riluzole protects against cardiac ischaemia and reperfusion damage via block of the persistent sodium current. *British Journal of Pharmacology, 160*, 1072–1082.

Wolf, J. A., Stys, P. K., Lusardi, T., Meaney, D., & Smith, D. H. (2001). Traumatic axonal injury induces calcium influx modulated by tetrodotoxin-sensitive sodium channels. *Journal of Neuroscience, 21*, 1923–1930.

Yuen, T. J., Browne, K. D., Iwata, A., & Smith, D. H. (2009). Sodium channelopathy induced by mild axonal trauma worsens outcome after a repeat injury. *Journal of Neuroscience Research, 87*, 3620–3625.